What the landscape can tell: An integrative stratigraphic prospection approach for localizing a Black Death mass grave in Erfurt/Central Germany

Michael Hein[1,2,3*], Nik Usmar[2], Annabell Engel[4], Johannes Rabiger-Völlmer[2], Johannes Schmidt[1,2], Matthias Silbermann[5,6], Marco Pohle[5], Iris Nießen[1,7], Martin Offermann[1,2], Lukas Werther[7,8], Birgit Schneider[2], Christian Tannhäuser[9], Alexander Herbig[10], Jan Nováček[11], Ulrike Werban[5], Martin Bauch[4], Christoph Zielhofer[1,2]

[1]Historical Anthropospheres working group, LeipzigLab, Leipzig University, Germany)

[2]Physical Geography, Institute for Geography, Leipzig University, Germany

[3]Institute of Ecology, Leuphana University Lüneburg, Germany

[4]Leibniz Institute for the History and Culture of Eastern Europe (GWZO), Leipzig, Germany

[5]Department Monitoring and Exploration Technologies, Helmholtz Centre for Environmental Research (UFZ), Leipzig, Germany

[6]Applied Near-Surface Geophysics and Remote Sensing, Institute for Earth System Science and Remote Sensing, Leipzig University, Germany

[7]Department for Medieval Archeology, Institute of Prehistory, Early History and Medieval Archeology, Eberhard Karls University, Tübingen, Germany

[8]Romano-Germanic Commission, German Archeological Institute, Frankfurt/Main, Germany

[9]Department for Cities, Thuringian State Department for the Preservation of Monuments and Archeology (TLDA), Weimar, Germany

[10]Department of Archeogenetics, Max Planck Institute for Evolutionary Anthropology, Leipzig, Germany

[11]Department of Anthropology, Thuringian State Department for the Preservation of Monuments and Archeology (TLDA), Weimar, Germany

*Corresponding author

E-mail addresses: m.hein@uni-leipzig.de, nikusmar@gmx.de, annabell.engel@gmx.de, j.rabiger-voellmer@uni-leipzig.de, j.schmidt@uni-leipzig.de, matthias.silbermann@uni-leipzig.de, marco.pohle@ufz.de, iris_ophelia.niessen@uni-leipzig.de, martin.offermann@uni-leipzig.de, lukas.werther@uni-tuebingen.de, bschneid@rz.uni-leipzig.de, Christian.Tannhaeuser@tlda.thueringen.de, alexander_herbig@eva.mpg.de, Jan.Novacek@tlda.thueringen.de, ulrike.werban@ufz.de, martin.bauch@leibniz-gwzo.de, zielhofer@uni-leipzig.de

Peer review status:

This is a non-peer-reviewed preprint submitted to EarthArXiv. The manuscript is also under review at PLOS One.

Abstract

The Black Death pandemic (1346-53) has caused a 30-50% population decline across Europe. For the city of Erfurt in Thuringia, substantial human losses and corresponding mass graves are well-documented in historical archives. The aim of our study is to localize these mass graves in the deserted village of Neuses in order to validate the written sources and to obtain skeletal remains for future anthropological and archeogenetic analyses. Here we present our integrative approach of historical research and minimally-invasive pedostratigraphical and geophysical prospection. Within the area of interest, narrowed down by historical accounts and GIS implementations, we applied vibracoring and electrical resistivity tomography (ERT). Coupled geophysical and coring sections help elucidate the late Quaternary sedimentary processes as an essential natural background for more detailed geoarcheological prospections. They allow for the designation of two distinct pedogeographical zones with consistent stratigraphical and pedogenic sequences: (1) a *Chernozem* zone and (2) a *Black Floodplain Soil* zone. The distribution and extent of these zones co-determined the internal structure of the former village Neuses and the positioning of the presumed associated Black Death mass graves. Our approach enabled a preliminary reconstruction of the medieval subsurface architecture, despite large-scale 20th century ground modifications. We identified a belowground pit structure visible both in the borehole sequences and ERT sections. Recovered bones have been AMS radiocarbon dated to the 14th century. Seeing as confirmed and precisely dated locations of Black Death mass graves are rare in Europe and are commonly found by chance during construction works, our planful discovery may help to advance the research on the origin, spread and evolution of the *Yersinia pestis* pathogen throughout this pandemic as well as societal coping mechanisms during epidemic outbreaks. Furthermore, our method combination holds the potential to successfully resolve the mapping of similarly demanding sites for archeological and forensic investigations.

1. Introduction

1.1 Cause and effect of the Black Death

The Black Death (1346-1353), the onset of the Second Plague Pandemic, was the single most destructive disease in Eurasian history. Its demographic toll is estimated at 30 to >50% of the European population (1,2), albeit with considerable regional variation (3). Only quite recently, the bacterium *Yersinia pestis* was unambiguously identified as the causative agent of the Black Death. Rodent populations are thought to have acted as the resident hosts for *Yersinia pestis* before the spillover to humans occurred mainly via infected fleas (4,5). The pandemic originated in Central Asia in the first half of the 14th century (6,7) and found its way to Western Eurasia through the Black Sea region and Mediterranean harbors, likely disseminated along cereal trade networks (8–10). It is still a matter of debate, whether and to what extent the emergence and the transmission of the pathogen were affected by climatic conditions (4,11).

1.2 Evolution of the Second Plague Pandemic

The Black Death was only the first wave of the Second Plague Pandemic, however, and the disease periodically returned to the European scene for centuries to come (12,13). While the genetic variety of *Y. pestis* was initially low during the Black Death, the bacterium diversified into multiple strains during the course of the Second Plague Pandemic (14–16). It is currently under discussion, whether the plague was reintroduced to Europe in the following waves (11,17) or reemerged from Central European reservoirs and then spread in concentric waves across the continent (18). With aDNA evidence drawn from investigations near Halle/Saale (19) and historical sources for Frankfurt and Thuringia (20), Central Germany is one plausible candidate region for hosting such reservoirs.

1.3 Historical and archeological perspectives

It is, however, equally true for Central Germany as for most other regions, that the vast majority of information on the Black Death is taken from documentary evidence provided by qualitative and

quantitative historical studies (2,17,20), whereas archeological material and complementary chronological data remain comparatively sparse (3,21). Historical sources imply numerous mass graves for plague victims dispersed throughout Europe (22,23). Yet, to our knowledge, there are altogether less than ten excavated European mass grave sites for which archeological and documentary evidence allow for precise dating to the period of the Black Death and for which positive identifications of *Y. pestis* were presented. Among them are Saint-Laurent-de-la-Cabrerisse and Toulouse/France, London East Smithfield, Hereford Cathedral and Thornton Abbey/England, and Barcelona/Spain (16,21,24–28), with the best-researched and most-precisely dated of these arguably being East Smithfield (25). For a couple of further mass grave sites with reference to the Black Death, such as Bergen op Zoom/Netherlands, Lübeck and Manching/Germany, as well as Kutná Hora/Czech Republic, either the chronology is still rather vague or the recorded mass fatalities were not unambiguously caused by *Y. pestis* (26,29–31). Apart from an undisputed potential for archeogenetic and anthropological studies, the very existence of a mass grave is a crucial piece of evidence for historical sciences as it testifies to a society that fell into disarray for its inability to bury the victims during an abrupt mortality crisis (23,32,33).

1.4 Mass graves: Modes of discovery

The significant scientific value of Black Death mass graves and their sizable numbers attested in historical sources stand in harsh contrast to their low archeological representation. Hence, the exploration for undiscovered sites is imperative not only for expanding the immediate data base, but also, their mapping and delineation can facilitate sustainable heritage management (cf. 34). By default, mass burials associated with the Black Death tend to be discovered by chance during construction works (25,26,29,35). Well-established geophysical methods, such as Electrical Resistivity Tomography (ERT) and Ground-Penetrating Radar (GPR), are often subsequently applied to characterize those features and to determine their extent (21,36). Systematic surveys for unmarked mass graves are, however, relatively rare in this archeological context (but see 34,37,38). Complementarily, a lot of research has been done on the detection of recent, i.e., clandestine mass graves for evidential and

forensic reasons, reviewed in Hunter and Cox (39). For such investigations, a stepwise approach is regularly used including (i) a map- and remote sensing-based background analysis, (ii) terrestrial reconnaissance utilizing a combination of several geophysical methods (e.g., ERT, GPR and fluxgate gradiometry), and eventually (iii) more extensive on-site investigations with excavations (cf. 40–44). The morphological prominence of older mass graves in their landscape might often be negligible or blurred through time, so that subsurface analysis is usually the only way for their detection. Conveniently, the backfill of a mass grave is likely to stand out from its environment by differences in texture, color, moisture, elemental and organic matter contents, or some combination thereof. For that very reason, it can e.g. be detected by geophysical means (33). In spite of these unique sedimentary properties, soil mapping and sediment coring to unravel the natural stratigraphy of the surroundings and to compare it with potentially deviating structures is not a common part of a systematic prospection concept for mass graves, historical or otherwise. However, we argue that this kind of stratigraphic exploration should be an integral component for locating mass graves and similar subterranean features, at the very least in order to facilitate optimal interpretation and contextualization of geophysical results.

In case of the city of Erfurt, a major medieval urban center, we have particularly good prerequisites to combine methods of historical, archeological and geophysical research: According to a contemporary local chronicle, the onslaught of the Black Death began in the summer of 1350 (20), killing thousands of its inhabitants. Most of the dead were buried within eleven ditches in the parish churchyard of Neuses, a village some kilometers outside the city (45–47). Earthworks to build Erfurt's first airfield in 1926/27 uncovered partial remnants of the former parish church along with one mass grave (45). Unfortunately, the documentation of the excavation and particularly the locational reference is rather inconclusive. It only exists fragmentarily in local archives and none of the skeletal remains are preserved.

1.5 Research objectives

In order to obtain verifiable chronological, archeological, archeogenetic and anthropological evidence for Black Death mass graves in Erfurt, it is mandatory to first track down their exact location. The manyfold references for a large-scale emergency burial at that time from written sources, images, inscriptions and tentative archeological findings together with the situation of Erfurt within a wider plausible candidate region for the reemergence of the plague following the Black Death, highlight the potential and significance of this endeavor. After all, subsequent plague waves from the mid-14th century onwards are well-documented for the city, as well (20). Here we present the results of our multi-phased and comprehensive survey strategy to detect and characterize the Black Death mass grave(s) of Erfurt/Neuses using combined geophysical and pedostratigraphical prospection methods. Our objectives were to 1. narrow down the suspect area for the presumed Black Death mass graves, 2. explore the natural stratigraphic and pedogenic setting by means of sediment coring and geophysical surveys to generate a broader contextual understanding of the site, 3. specify the best-suited geophysical methods for the detection of a mass grave and characterization of the natural background alike, 4. supplement the existing historical and preliminary archeological record with independent chronostratigraphic evidence and 5. locate the mass grave(s) as a basis for a future excavation and to further archeogenetic and anthropological investigations.

2. Materials and Methods

2.1 Natural setting of the study area

The city of Erfurt (50°59'N, 11°2'E) is situated in Central Germany (Fig. 1A), within the southern part of the Thuringian Basin (Fig. 1B). Shales and mudstones from Upper Triassic Keuper period generally dominate the interior of the Thuringian Basin, shaping gently undulating landscapes (48). The area of interest (AOI: Figs. 1C/D) is positioned at the southeastern footslope of the hill "Roter Berg" ("Red Mountain"), a prominent erosional remnant made up of mainly reddish shales and mudstones from the Middle Keuper (Norian Stage in the Upper Triassic Epoch) surrounded by fluvial gravels of the Weichselian

(Upper Pleistocene) Lower Terrace in the wide Pleistocene valley of the River Gera. On the hill's flat summit, a small veneer of highly-weathered fluvial gravels related to the late Elsterian Upper Middle Terrace is preserved. The vertical distance between the two terrace surfaces amounts to ~50 m. In some areas, the Lower Terrace bears a ca. 2 m thick cover of loess and loess derivates, in which Chernozem-like soils developed during the Holocene. Where this loess cover is missing, especially south and southwest of the "Roter Berg", loamy soils formed through weathering of the Lower Terrace gravels (Thuringian State Office for the Environment, Mining and Nature Conservation; Fig.1C/D). In these loess-free areas of the Lower Terrace occurring in the southern part of the AOI, wetlands existed at least until the 19th century (SI Fig. 1A).

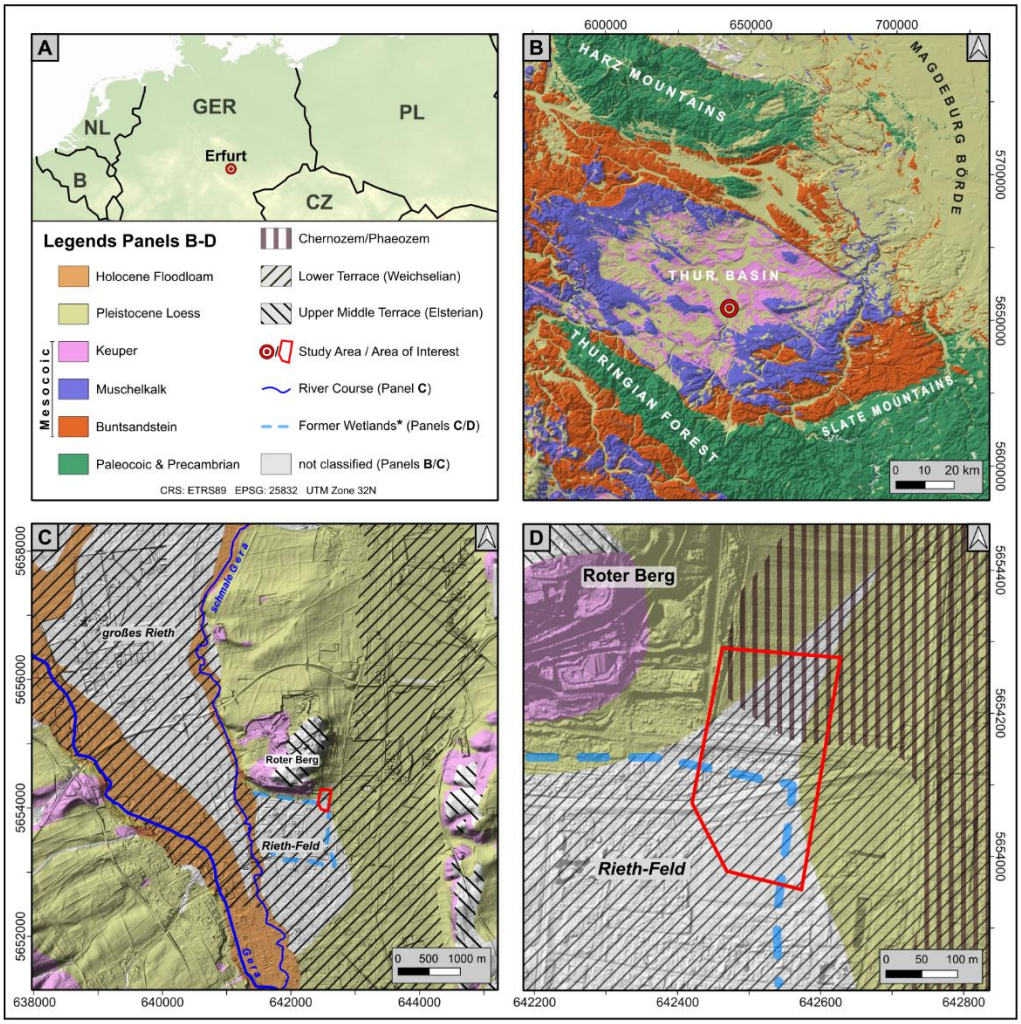

***Fig. 1**: Geographical, topographic and geological overview of the study area. Its position is given within (**A**) Central Europe, (**B**) the Thuringian Basin, (**C**) within the wide valley now partially occupied by the river Gera and (**D**) at the SW footslope of the hill "Roter Berg". Topographic information in panels A and B obtained using open-access SRTM data with a 90-m resolution (www.earthdata.nasa.gov/sensors/srtm). For panels **C** and **D**, a LiDAR Digital*

*Elevation Model DEM1 with 1-m resolution was used, kindly provided by the Thuringian State Office for Land Management and Geoinformation. Geological information, according to the German Stratigraphic Commission taken from the Digital Geological Map GK25; pedological information taken from the soil map BGK 100. Both were kindly provided by the Thuringian State Office for the Environment, Mining and Nature Conservation. *The rough area of former wetlands was deduced from older topographic and geological maps from 1839 and 1932, respectively (see Supplementary Section 1).*

The potential natural vegetation consists of *Fraxinus-Carpinus* to *Tilia cordata-Fagus* forest, depending on the kind of substrate (49). Today, the AOI has a roughly three-part structure in terms of vegetation cover (SI Fig. 3). Its northern part is used for agriculture with dominant wheat and rapeseed cultivation, the middle part features a dense, partly spontaneous forest with *Populus*, *Acer*, *Sambucus* and *Prunus* species, while the southern part is occupied by a sports facility. Due to the shielded topographic location in the Thuringian Basin, Erfurt has low overall precipitation values of 530 mm/a with a pronounced summer maximum, and an average annual temperature of 9°C. According to the Köppen-Geiger classification, the region is located within the Dfb climatic zone (50,51).

2.2 Archeo-historical setting of the study area

A first reference to the existence of plague mass graves in the deserted village of Neuses at the foot of "Roter Berg" is given in the *Chronicon Sampetrinum* (46), a chronicle which covers the history of the St. Peter monastery in Erfurt from 1072 to 1355 and is hence considered a contemporary source of local information (52). The chronicle describes the overflow of Erfurt's parish cemeteries with the outbreak of the Black Death and the advice of academics to dig ditches instead. To accommodate the growing number of bodies, the cemetery of the nearby village of Neuses, probably still in use for the local parish, was chosen by official decree as an emergency burial site. There, between July 1350 and February 1351, "eleven pits were dug […], into which around twelve thousand bodies of people were brought in wagons and carts. These were continuously transported, three or four at a time" (53). In the immediate aftermath, but at least since 1355, an annual commemorative procession was established on St. Mark's Day (April 25th), leading from Erfurt to the mass graves in Neuses (20, footnote 57), which was upheld for several centuries.

In 1926/27, large-scale ground modifications and terrain levelling took place in the AOI for the construction of Erfurt's first airfield (see Fig. 2A). On the northern margin of the prospective runway, traces of the medieval deserted settlement of Neuses were discovered and partly excavated. These results were presented alongside historical source studies in two publications by Bolle (45,54). The findings include the former churchyard with individual graves as well as the presumed debris of the former parish church and remains of the cemetery wall. A 1.50 m by 1.50 m test pit on a slight hillock there revealed a mass grave at 1.30 m below the surface, featuring human skeletal remains of ca. 20 individuals stacked upon each other without discernible organization or orientation, and apparently buried without a coffin. At a depth of 2.50 m, the excavation was suspended, although the bottom of this structure had not been reached. Based on the written sources, Bolle (45) related this archeological feature to one of the supposed eleven Black Death mass graves from 1350/51. Unfortunately, the current whereabouts of these skeletal remains are unknown, preventing their use for dating or other purposes. Therefore, a deviating chronology of this previously found mass grave cannot yet be excluded, e.g., the Thirty Years War or the prehistoric period, with the latter being extensively represented in the immediate vicinity (32,45,55).

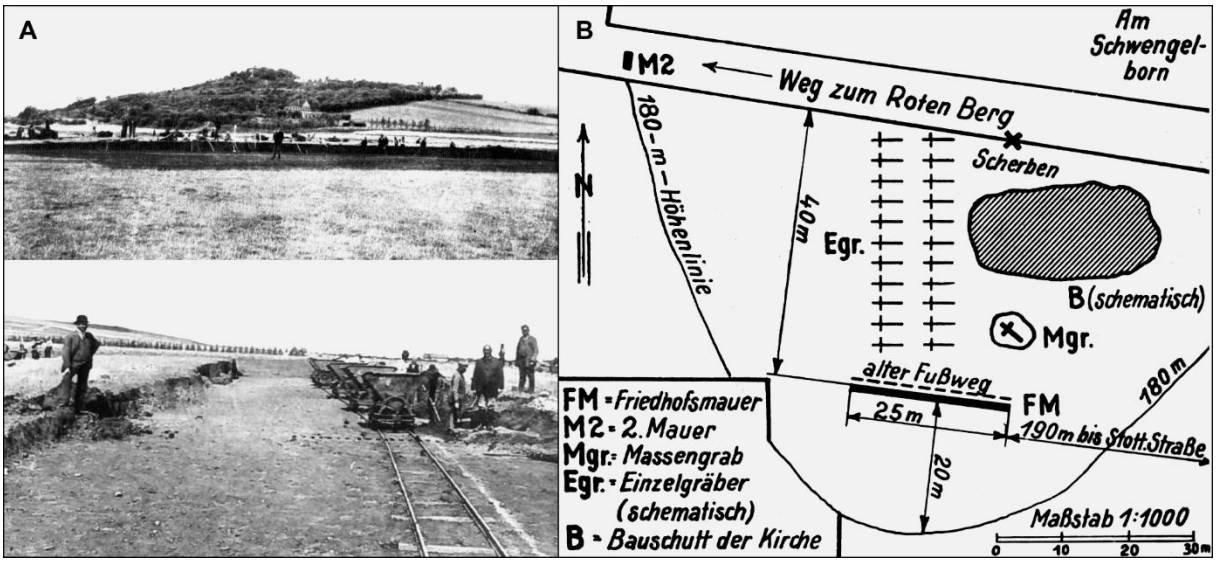

***Fig. 2: Panel A** - Terrain levelling for the construction of the airfield in 1926 with the hill "Roter Berg" in the background (courtesy of Thuringian State Department for the Preservation of Monuments and Archaeology TLDA; photo credits: Wilhelm Lorenz 1926). **Panel B** - Sketch of the excavation findings 1926/27 (Bolle, 1937). For positioning, the sketch includes a scale (lower right) and the directional distances to the nearest roads. Abbreviations: **FM**=cemetery wall, **M2**=second wall, **Mgr**.=mass grave, **Egr**.=individual graves (schematic), **B**=debris of the former church (schematic).*

2.3 Geoinformatics and geodata management

The two reports on the preliminary results of the 1926/27 excavation also contain a sketch locating Neuses within the rural landscape, and a detailed scaled map of the excavation area showing the locations of the churchyard, cemetery and mass grave. Their spatial relationships and distances to adjacent roads and footpaths are also indicated (45,54, Fig. 2B). However, this map merely represents a vague starting point for the actual localization of the mass grave, because (i) the road network had been altered by the airfield construction itself and has evolved ever since, (ii) the excavation map is lacking a coordinate system and the section is too small-scale to refer it to any official streetmap, (iii) much of the spatial reference in the map consists of archeological features that have been eradicated due to the excavation itself and (iv) the original report and documentation of the excavation activity have not been preserved, so that the map cannot be critically evaluated and adjusted if necessary.

Therefore, we attempted to georeference the map in ESRI Arc GIS (version 10) using a tentative and exploratory approach (cf. 56) anchored on the few spatial specifications considered reliable in the excavation map (see SI Fig. 2 and Supplementary Section 2). This resulted in the preferential geographic positioning of the excavation sketch by Bolle and its major elements, as presented in Figure 3. However, due to a scarcity of suitable control points on this sketch, we concede that the easting (i.e. the accuracy on the west-east axis) remains a rather rough approximation. We further employed GIS to visualize the topographic data alongside geological and pedological information (source: Thuringian State Office for the Environment, Mining and Nature Conservation). Geophysical profiles and sediment cores attained during our fieldwork have been levelled with a TOPCON differential GPS (DGPS; cm-scale horizontal and vertical accuracy).

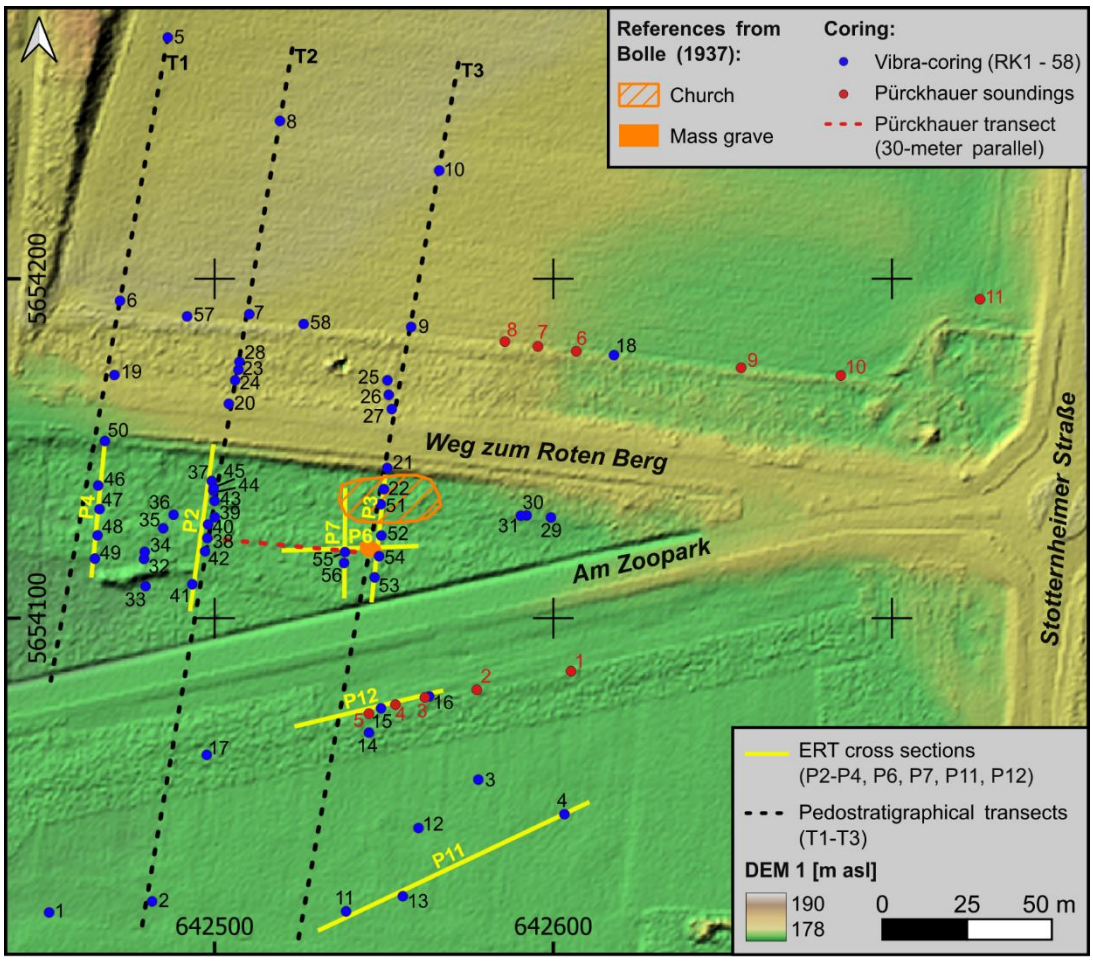

Fig. 3: *Digital elevation model of the study area displaying all coring positions (vibracoring and Pürckhauer soundings) and the course of all ERT-profiles included in the study (P2-P4, P6, P7, P11, P12). Also indicated in orange is the tentative position of notable features from the excavation in 1926/27 according to our preferential georeferenced version of the sketch by Bolle (1937), cf. Supplementary Section 2.*

2.4 Survey and prospection methods

2.4.1 Principal approach

To account for the challenging nature of mass graves with very individual sedimentary and dimensional properties and thus geophysical responses (33,cf. 43), we applied an integral combination of non-invasive and minimally-invasive survey and prospection techniques. Due to dense woody vegetation in vast parts of the AOI (SI Fig. 3), an extensive surface coverage was not applicable for the geophysical surveys. Therefore, the prospection strategy pursued a two-step approach. Firstly, ERT cross-sections and coring were carried out mainly along three approximately North-South-oriented transects T1 to

T3 (Fig. 3), carefully cut into the vegetation. Transects T2 and T3 were laid out to also intersect with the supposed position of the mass grave, depending on the respective variant of georeferencing the excavation sketch made by Bolle (45, see Fig. 3). By deliberation, our geophysical and coring profiles extent well beyond the narrowed-down suspect area for the mass grave. That way, we facilitated a better characterization of the natural setting and hence a wider contextual understanding of the mass grave site (cf. 34). Once this was achieved, we secondly made use of the fact, that in the old excavation sketch, the distance of c. 30 m from the supposed mass grave to the road "Weg zum Roten Berg" might be the most dependable piece of spatial information (Figs. 2, 3). Accordingly, our subsurface investigations were then turned to the parallel line 30 m south of the road, running roughly in a W-E direction, i.e., about perpendicular to most of the remaining profiles.

2.4.2 Near-surface geophysical methods

The application of geophysical methods is well-established for the detection and mapping of graves, where often a preference is given to electrical and electro-magnetic approaches (36,44,57). Due to dense vegetation and thus transect-wise mapping we had to refrain from using electromagnetic induction methods as an option for area-covering investigations. We focused on electrical resistivity tomography (ERT) that measures apparent electrical resistivity distribution in the subsurface with high vertical resolution. ERT is quite commonly used to investigate substrate variations (58) and moreover was successfully applied to map changes of bulk density caused by mass graves (36). ERT profiles were measured with a PC-controlled direct current resistivity meter system (Resecs II, GeoServe, Kiel, Germany). Electrode spacing was 0.5 m and transect length varied from 37 to 87.5 meter. Figure 3 shows the spatial layout of our ERT surveys. We chose a Wenner electrode array because of its low signal-to-noise ratio and appropriate vertical resolution for mapping the transects that focus on the stratigraphical background (transects P2, P3 and P4). Measurements were performed in September 2022 after a very dry summer period. For transects that aimed to image possible grave structures itself (transects P6 and P7), we applied Wenner- and additionally Dipole-Dipole electrode configuration in order to allow for higher lateral resolution. Transects P6 and P7 were measured in January 2023 under wet

surface conditions. Transects P11 and P12 were measured in the beginning of June 2023. The data were processed and inverted using boundless ERT (BERT) software (59). We opted for L1 norm for inversion and the smoothing parameter was set to $\lambda = 20$ to $\lambda = 80$.

Ground penetrating radar (GPR) was tested along several transects across the AOI. The penetration depth and resolution of GPR depends on electrical conductivity, dielectric permittivity, and magnetic permeability of the underground material (60). Measurements were performed with an SIR-4000 (GSSI Geophysical Survey Systems, Inc., Nashua, USA) and antenna frequencies from 200 MHz up to 800 MHz (UtilityScan DF 300/800, 200 MHz and 400 MHZ – Shielded Antenna, GSSI Geophysical Survey Systems, Inc., Nashua, USA). Due to the strong presence of clay (floodplain and colluvial sediments) in the first centimeters we are dealing with a very high attenuation and a very low penetration depth (61). GPR was therefore unsuitable for our field site.

2.4.3 Pedostratigraphic survey

We conducted vibracoring (58 cores with $\leq$ 6m depth, Fig. 3) to establish the natural pedological and stratigraphic background along transects applying the soil catena concept (62). We utilized an Atlas Copco Cobra motor hammer and several 1-m long stainless-steel gouges with a diameter of 6 cm for coring. Borehole sequences were documented in the field following the standards of German soil mapping and the World Reference Base for Soil Resources, WRB (63,64). The descriptions comprise parameters such as bedding, texture, Munsell color, contents of humus, carbonates and clastic coarse fraction, redoximorphic properties as well as anthropogenic constituents such as pottery sherds, brick fragments and charcoal. Compared to this natural reference, sediment sequences or segments that are conspicuous with respect to multiple of these parameters could indicate anthropogenic sub-surface disturbances. In addition to vibracoring, Pürckhauer soil probes were used for time-efficient subsurface prospection. These 1-m long notched metal rods were driven into the ground by hand with a 3 kg plastic hammer. Pürckhauer sequences were not fully documented, because when deviations or anomalies occurred, they were instantly double-checked through vibracoring.

2.5 Dating approaches

2.5.1 Radiocarbon dating

Bone fragments and four additional charcoal pieces from the sediment cores have been subjected to AMS ^{14}C dating at the Curt-Engelhorn-Zentrum Archäometrie (CEZA) in Mannheim (see Supplementary Section 5 for lab codes and analytical details). The bones were subjected to collagen extraction (modified Longin method) and ultrafiltration was used to separate the fraction >30kD, which was subsequently freeze-dried (65). On the charcoal pieces, the ABA protocol (Acid-Base-Acid) was performed using HCl, NaOH and HCl to eliminate the most probable contaminants (66). After pretreatment, the remaining sample residue was combusted to CO_2 in an elemental analyzer (EA) and the CO_2 was catalytically reduced to graphite. The ^{14}C content of the graphite was then measured applying a MICADAS-type AMS system. Simultaneously, $^{14}C/^{12}C$ and $^{13}C/^{12}C$ isotope ratios of samples, as well as calibration standards (oxalic acid-II), blanks and control standards were analyzed in the AMS. The determined ^{14}C ages were normalized to $\delta^{13}C$=-25‰ (67) and calibrated to calendar ages using the IntCal20 data set and OxCal software v4.4.2 (68).

2.5.2 Pottery-based chronological assessment

From the cores EN-RK 25, 27, 32, 35, 38, 46-48 and 57, we collected a total of 14 pottery sherds, mostly embedded within deposits classified as occupation and floodplain layers (Supplementary Section 3). The sherds were described with regard to the following optically analyzed characteristics: State of preservation, production technique, color, firing atmosphere, temper, hardness, surface texture and vessel type. Due to the strong fragmentation of all pieces, only a rough chronological classification could be made on the basis of the respective characteristics, as essential features such as rim and vessel shapes were generally not identifiable. Categorization was based on expert knowledge and the relevant overview literature (69–71). Further details can be found in the Supplementary Section 5.1.

2.6 Anthropological description of bones

Bone fragments discovered during the coring campaign have received an inventory number from the Anthropology Department of the Thuringian State Department for the Preservation of Monuments and Archeology (TLDA). All bones were characterized with regard to species, skeletal region, approximate age at death and sex (see SI Tab. 2).

3. Results

3.1 Stratigraphy and pedogeography of the study area

Pedogeographically, the study area can be divided into a northeastern part and a southwestern part with distinctly different near-surface depositional and pedogenic properties: a *Chernozem zone* and a *Black Floodplain Soil zone*, with the contact boundary of these two running right through the AOI. Figure 5 shows the affiliation of each coring location to one of these zones. Standardized sequences and the main stratigraphic units (SU) for both zones are presented in the following paragraphs, as well as Table 1 and Figure 4. More detailed litho- and pedostratigraphic information including references and argumentation for their interpretation can be found in the Supplementary Sections 3 and 6. Deviating and anomalous stratigraphic phenomena are also compiled there.

3.1.1 Standard stratigraphies

***Tab. 1**: Characterization of the Stratigraphic Units (SU) encountered in the study area. The occurrence of the SU within respective sediment cores and their affiliation with the two pedogeographical zones 'Chernozem zone' (CZ) and 'Black Floodplain Soil zone' (BFZ) is indicated.*

Strat. Unit	Core EN-RK	Thickn. [cm]	Main Sediment Characteristics	Resistivity in ERT	Interpretation	Pedo-Zone
SU1	1,32,33, 36,41, 55,58	tens of *meters*	unconsolidated (silty) clay; variegated colors (Munsell from 10R 5/2 and 2,5YR 4/3 to 6/5 BG); (vastly) non-calcareous; massive to finely-laminated and free of pebbles; clear and erosional upper boundary	low values < 60 Ωm	mudstone from the *Middle Keuper* (Weser formation)	**CZ, BFZ**
SU2	3,4,7,19 36-38,40, 42,51, 53,55-58	~200	gravelly, poorly-sorted fine to coarse sand; pebbles well-rounded; gravel content 10-50 % (mainly quartz, chert, rhyolite and limestone); varyingly calcareous (1 to 10 %); mostly reddish-brown color (between 5YR 5/2 and 5/5), clear upper boundary	high values ≤ 400 Ωm	*Weichselian* fluvial gravel of the 'Lower Terrace', German: "Niederterrasse"	**CZ**
SU3	3-10,18-31,37-45, 50-58	90- >350	heterogeneous clayey loam; massive to finely-laminated; gravel content up to 15% (mainly quartz, rhyolite); carbonate content up to 10 %; mostly reddish brown (2,5YR 3/4 to 5YR 6/2); clear and erosional upper boundary	low to medium values 50-150 Ωm	*Weichselian* periglacial slope debris/deposit	**CZ**
SU4	3-5,7,9, 10,16,18-28, 51-54	20-90	alternate, rhythmic bedding and partial mixture of (clayey) reddish brown loam and light brown silt (7,5 YR 6/5 to 2,5YR 4/4), highly calcareous (5 to >10%); interfingering of SU3 and SU5.1 characteristics; gradual upper boundary	low to medium values 50-150 Ωm	*Weichselian* slope-washed loess, German: "Schwemmlöss"	**CZ**
SU5.1	3-10,16, 18,20-24, 26,28-31, 51,58	15-65	massive, (slightly fine-sandy to slightly loamy) silt; light (yellowish to reddish) brown (10YR 6/5 to 7,5YR 5/4); highly calcareous (≥10 %); contains krotovinas, earthworm channels and secondary carbonates; clear but gradual and contorted upper boundary	low to medium values 50-150 Ωm	*Weichselian* primary loess	**CZ**
SU5.2	3-10,15, 16,18,23, 24,26, 28,29,58	45-90	mostly massive humic/mollic, dark brown solum (7,5YR 3/2 to 10YR 3/3); granular structure (earthworm-casts); varying carbonate contents (0-10 %); occasionally incipient degradation into (luvic) phaeozem; contains krotovinas and earthworm channels; plough. horizon usually with Munsell values of 4	low to medium values 50-150 Ωm	*Holocene* chernic horizon	**CZ**
SU6	1,2,11-14, 17,32-35, 41,46-49	100-170	gravelly sand to sandy gravel; slightly loamy, fine to coarse sandy, poorly-sorted matrix with more loamy sections; variegated but mostly reddish colors (2,5Y, 10YR, 7,5YR, 5YR to mostly 2,5YR 6/3-5/2); calcareous (2 to >10 %); well-rounded pebbles (30-60 %), mainly quartz, chert and rhyolite, with higher limestone contents than SU2; sporadically with fining-up sequences; erosional lower boundary	high values ≤ 400 Ωm	*Late Weichselian* to *Early Holocene* fluvial gravel	**BFZ**
SU7	1,2,11-14, 17, 32-35, 41,46-50	70-120	massive, very humic, loamy-clayey solum/pedosediment (Munsell 7,5YR 2/1 to 2,5Y 3/1); clay content up to 50 %; sand fraction well-sorted medium to coarse sand; carbonate content 0 to 10 %; uppermost segments usually lighter and siltier; contains small pieces of charcoal and burnt loam; gradual lower boundary with decreasing clay and humus, but increasing carbonate content	varied, low to medium values 50-100 Ωm	*Early- to Mid-Holocene* organic to clastic overbank formation, poss. with weathering/ pedogenesis	**BFZ**

As the lowermost Stratigraphic Unit 1 (SU1) within the entire study area, we encountered a mudstone sequence from the Middle Keuper stage. In the ***Chernozem zone***, it is unconformably overlain by Stratigraphic Unit 2 (SU2), represented by fluvial gravels of the Weichselian Lower Terrace. This, in turn, is covered by a loamy periglacial slope deposit, Stratigraphic Unit 3 (SU3). Following an erosional

contact, Stratigraphic Unit 4 (SU4), a laminated slope-washed loess was deposited, which grades into a rather thin primary loess, Stratigraphic Unit 5.1 (SU5.1). Within this loess, a chernozem has formed at the surface, the chernic horizon designated as Stratigraphic Unit 5.2 (SU5.2). In the ERT-profiles (Fig. 6), SU1 and SU2 can be distinguished by their particularly low (less than 50 Ωm) and relatively high (300- 400 Ωm) resistivity values, respectively. In contrast, SU3 to SU5 show moderate resistivities of 60 to 150 Ωm, thus these units cannot be differentiated from each other on the basis of their resistivity alone (Tab.1; Fig. 6; Supplementary Section 3). Within the ***Black Floodplain Soil zone***, SU2 to SU5 are missing. Instead, with Stratigraphic Unit 6 (SU 6), a fluvial gravel of a presumed younger age than SU2 overlies the ubiquitous Keuper mudstone of SU1. On top of SU6, the uppermost Stratigraphic Unit 7 (SU7) is formed by a thick humic and loamy solum, bearing evidence for both, in-situ pedogenesis and the deposition as a pedosediment, i.e. overbank deposit. It is denominated as a Black Floodplain Soil. Resistivity values in the ERT profiles within this zone allow for a clear separation of SU1 (<60 Ωm), SU6 (≤400 Ωm) and SU7 (50 to 100 Ωm) (Tab.1 and Fig. 6; SI Fig. 4).

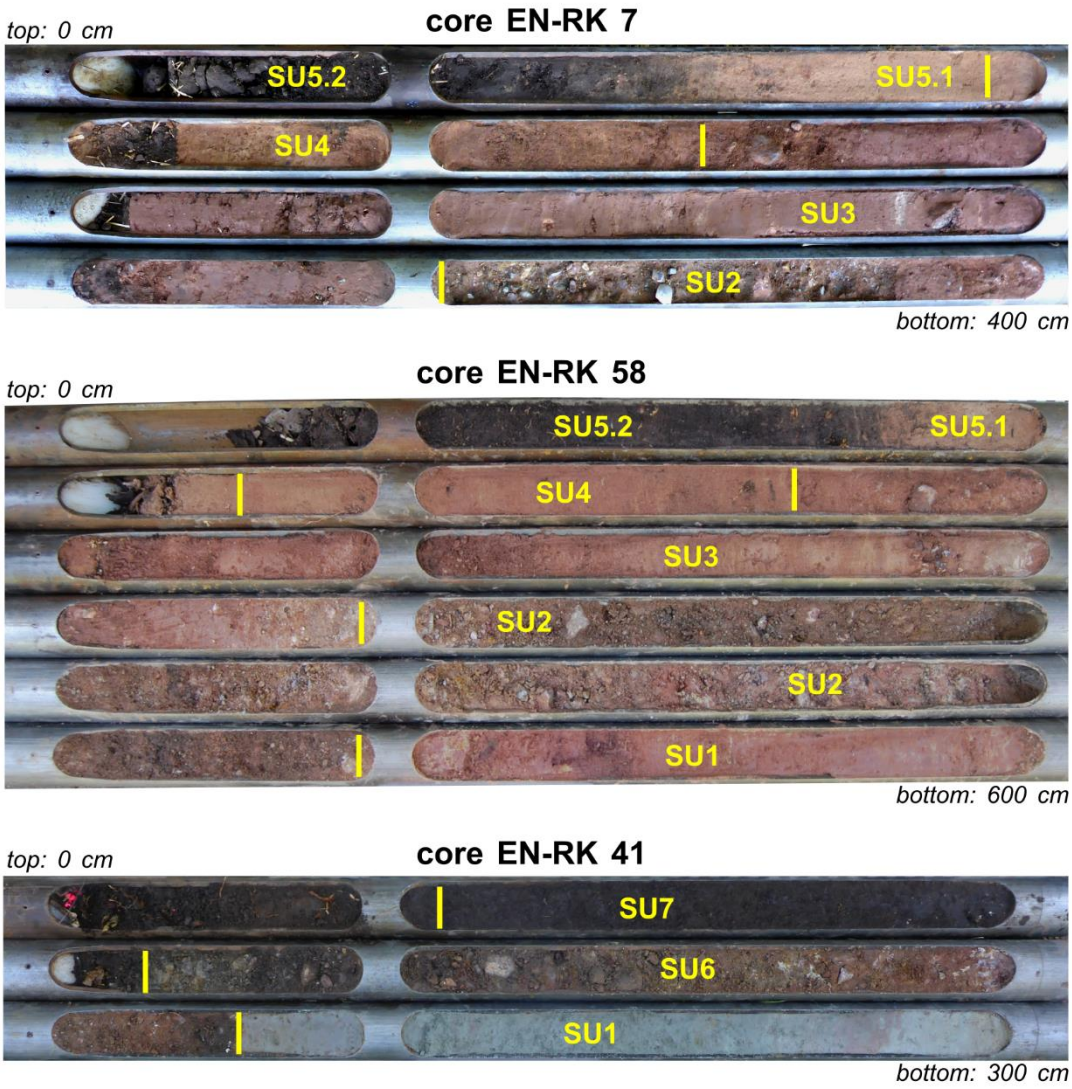

Fig. 4: *Photographs of cores representing the* ***Chernozem*** *standard sequences-(EN-RK 7 & 58) and the* ***Black Flood-plain Soil*** *standard sequence (EN-RK 41). The attribution of the different deposits to stratigraphic units (SU) is indicated. Descriptions of SU1 to SU7 can be found in Table 1 and Supplementary Section 3.*

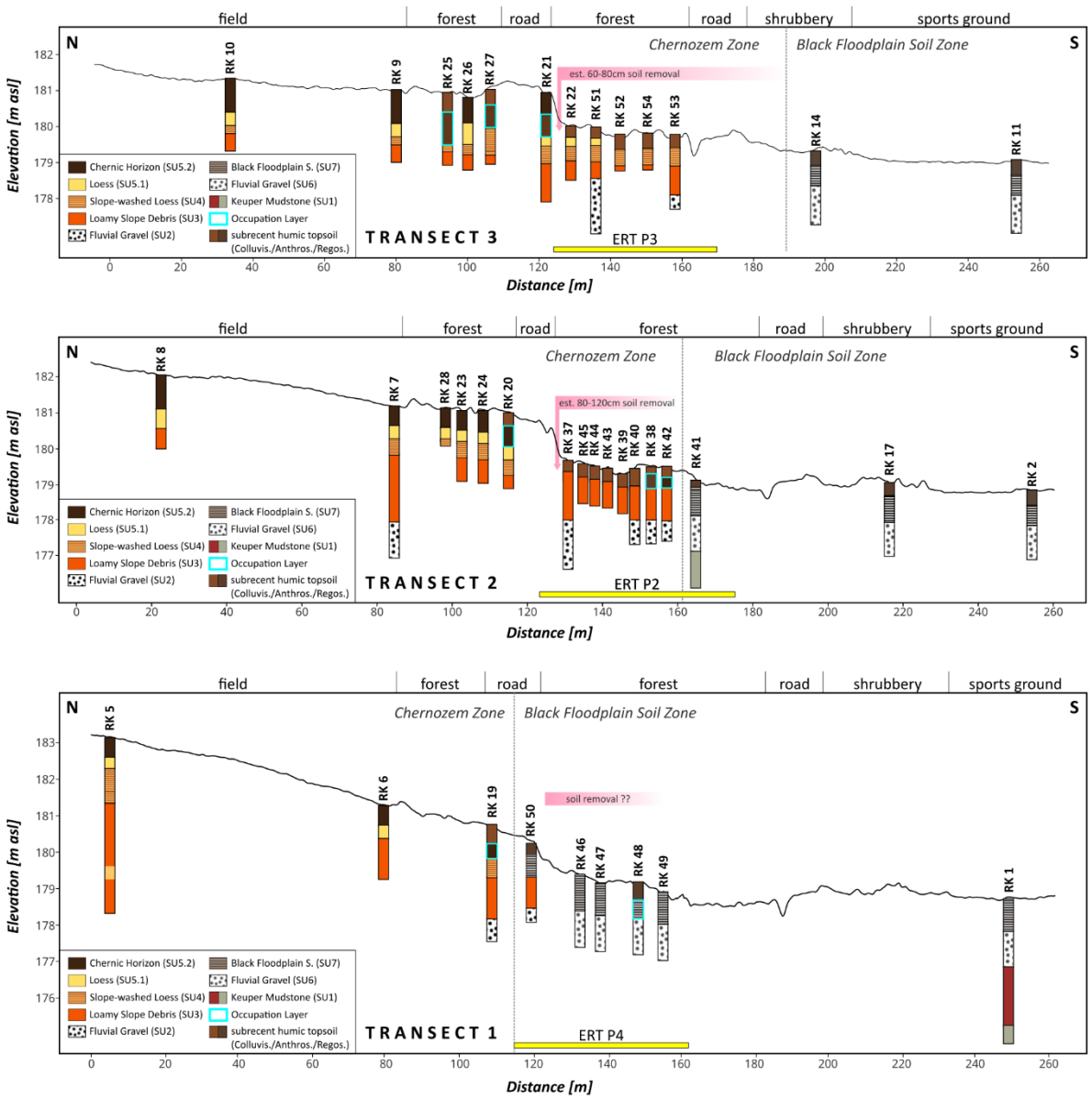

Fig. 5: *Simplified pedo- and lithostratigraphic sequences along the three coring transects T1 to T3 (Fig. 3). The boundary between the Chernozem and the Black Floodplain Soil zone is depicted. The estimates for truncation/soil removal in the central parts of the transects caused by ground modifications in the course of the airfield construction in 1926/27 are indicated by the pale pink rectangles. Yellow bars specify the segments covered by the respective ERT profiles.*

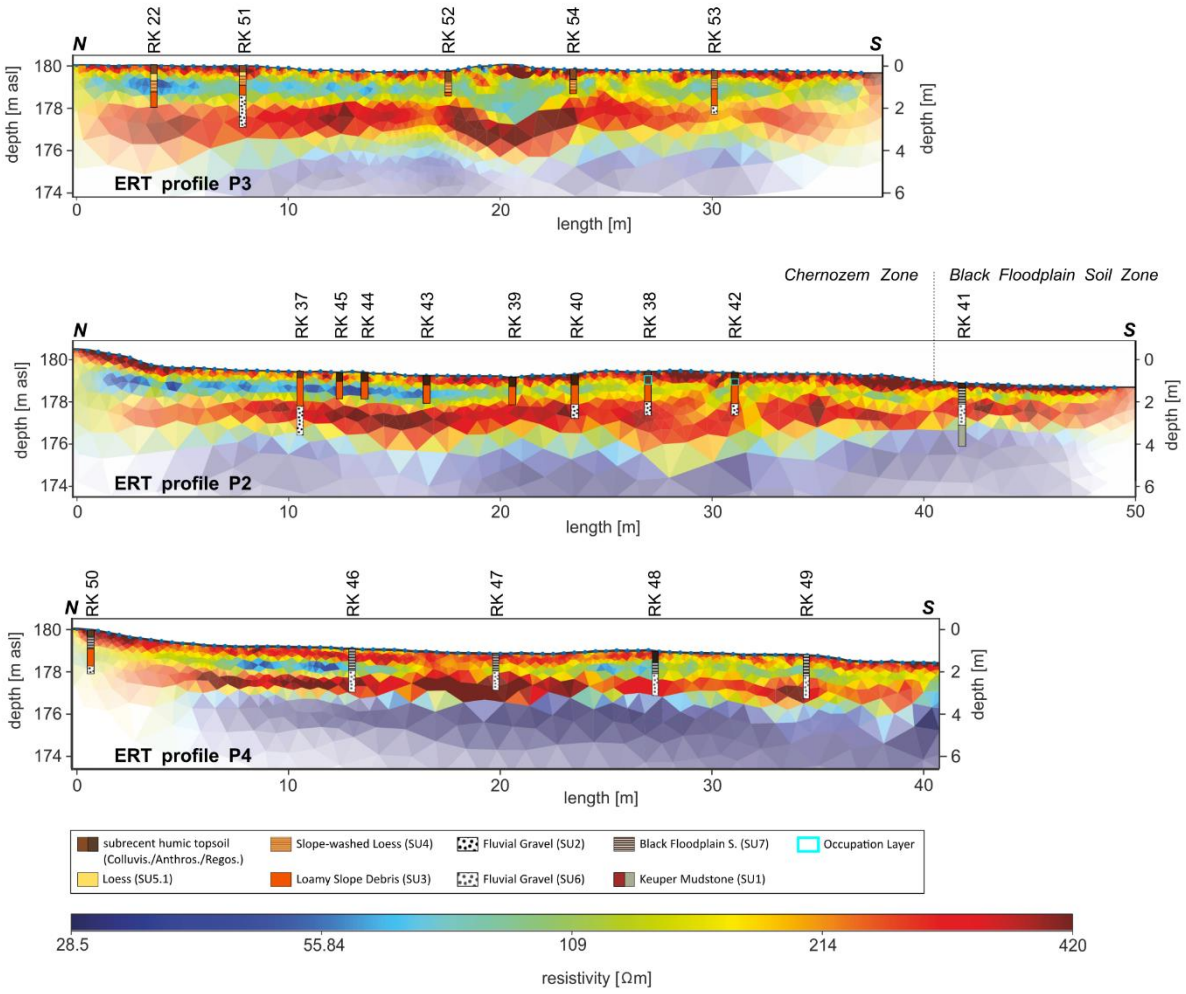

Fig. 6: *ERT-profiles P2 to P4 (electrode spacing of 0.5 m, model is based on an inversion of a Wenner configuration), arranged from east to west from top to bottom. The profiles are aligned with the central sections of the coring transects T1 to T3 (for positions see Fig. 3).*

3.1.2 Transect-related stratigraphic findings

The stratigraphic results along the three main coring transects T1 to T3 are shown in Figure 5, furthermore, the segments covered by ERT surveys are indicated (cf. Fig. 3). ERT profiles P2-P4, located in the forested central sections of T1-T3 are displayed in Figure 6. The northern parts of the coring transects, up to and including the embankment of the road “Weg zum Roten Berg”, show fairly consistent and similar stratigraphies. In almost every borehole in this area, stratigraphic units SU3, SU4 and SU5 are represented, although with slightly varying thicknesses. As a general trend, the slope deposits, i.e., the combined units SU3 and SU4, seem to thin out downslope. In a few positions,

however, SU4 does not occur (EN-RK 6 and 8), and SU5 is occasionally obscured by occupation features (EN-RK 19, 25, 27). South of the road, the lowering and levelling of the terrain for the former airfield created a morphological step and further resulted in a systematic truncation of the stratigraphic succession, especially in T2 and T3. The amount of intentional soil removal can cautiously be reconstructed based on the relative thickness of lacking stratigraphic units (Fig. 5). As for T1, the morphological step south of the road is less pronounced and it coincides with the transition from the Chernozem zone to the Black Floodplain Soil zone. At the contact of these two, a short-distance reworking of SU3 material has apparently taken place (EN-RK 50), as this is the only position, where SU7 is overlying SU3 in the whole study area. The amount of soil removal south of the road in T1 is difficult to assess, because the entire share of Black Floodplain Soils we studied so far is situated within the boundaries of the former airfield. Hence, the standard thicknesses of SU7 are currently not known to us and therefore, neither is the magnitude of a possible truncation. It is not unlikely that no or only negligible soil removal occurred in this range of T1 and that the step represents a largely natural landform feature here. The incongruent degrees of soil removal across our transects T1-T3 are clearly related to the original southward bulging of the topography prior to the airfield construction (see the 180 m contour line in Fig. 2). The slightly higher elevation in the center of the bulge required more extensive lowering to level the ground there. In the ERT profiles, stratigraphic units SU3-SU5 cannot be differentiated. However, the profiles clearly show the low-resistivity Keuper mudstone (SU1) at depths of 3 to 4 m in P2-P4, as well as the gravel of SU2 with higher resistivities and a respective thickness and depth of about 2 m. Since this is both corresponding with our coring results, it allows to infer a stratigraphic continuity of SU1 and SU2 even in segments where these units are only scarcely exposed through vibracoring (Fig. 6).

The southwestern part of the AOI and of our transects is occupied by the Black Floodplain Soil zone. While in T1 circa half of the overall boreholes are located there, in T2 and T3 its boundary with the Chernozem zone lies further to the south. In fact, a gradual southward shift of this boundary can be observed in the investigated area from west to east (Fig. 5), likewise visible in ERT (Fig. 6). As this

contact is utterly sharp and as the Black Floodplain Soil zone is unaffected by the deposition of SU3 to SU5, a formation of SU6 and SU7 after the loess accumulation must be presumed. Across this contact, in the ERT profiles, it is not possible to distinguish between the fine-grained capping deposits of the Chernozem Zone (SU3-SU5) and the Black Floodplain Soil zone (SU7) based on their resistivity values alone. The same is true for the two separate fluvial gravels (SU2 versus SU6). However, a clear distinction is facilitated by their relative stratigraphic properties: The capping deposits are much thinner in the Black Floodplain Soil zone and the gravels lie much closer to the surface compared to Chernozem zone. As these findings are well in accordance with the borehole stratigraphies, the contact between the two pedogeographic zones can be reliably mapped using ERT even in the local absence of a high vibracoring density. The contact is most pronounced in P11 (at ~45m), well-discernible in P2 (~41m), and has a more transitional character in P12 (~23 to 28m) (SI Fig. 4).

3.2 Systematic localization and characterization of the mass grave

According to our geographic positioning of the excavation sketch by Bolle (45), we expected the mass grave (Fig. 2, SI Fig. 2) to fall in line with transect T3 and ERT profile P3 (Fig. 3). However, we did not identify a corresponding feature there, which is likely caused by substantial uncertainties in the west-east direction of the control points for georeferencing. Therefore, given that the distance of ca. 30 meters between the road “Weg zum Roten Berg” and the presumed mass grave is its most dependable spatial reference on the sketch, we staked out a parallel line 30 meters south of the road, intersecting with our transects T2 and T3 (red dotted line in Fig. 3). Along this parallel line, we carried out shallow Pürckhauer soundings (depth: 100 cm) every two meters and increased the resolution if necessary. Equipped with an adequate understanding of the original stratigraphy, we focused on conspicuities and deviating properties in terms of color and texture and generally unusual constituents. The results of these Pürckhauer soundings mostly mirrored the vibracoring findings of the immediate surroundings: We encountered the loamy slope debris (SU3), occasionally with a thin overburden of slope-washed loess (SU4) in which a recent humic topsoil had formed. About 10 meters west of T3, however, we discovered a stratigraphic anomaly, characterized by a slightly elevated humus content

and the noticeable admixture of pebbles, as well as the occurrence of brick and charcoal fragments below the topsoil (Fig. 7A). As these properties are atypical for the SU3 deposits and were restricted to a very small section of this 70-meters long Pürckhauer transect, we further explored this anomaly through vibracoring and conducted ERT measurements in a cross-wise manner (P6 and P7) to outline the anomaly (Fig. 8).

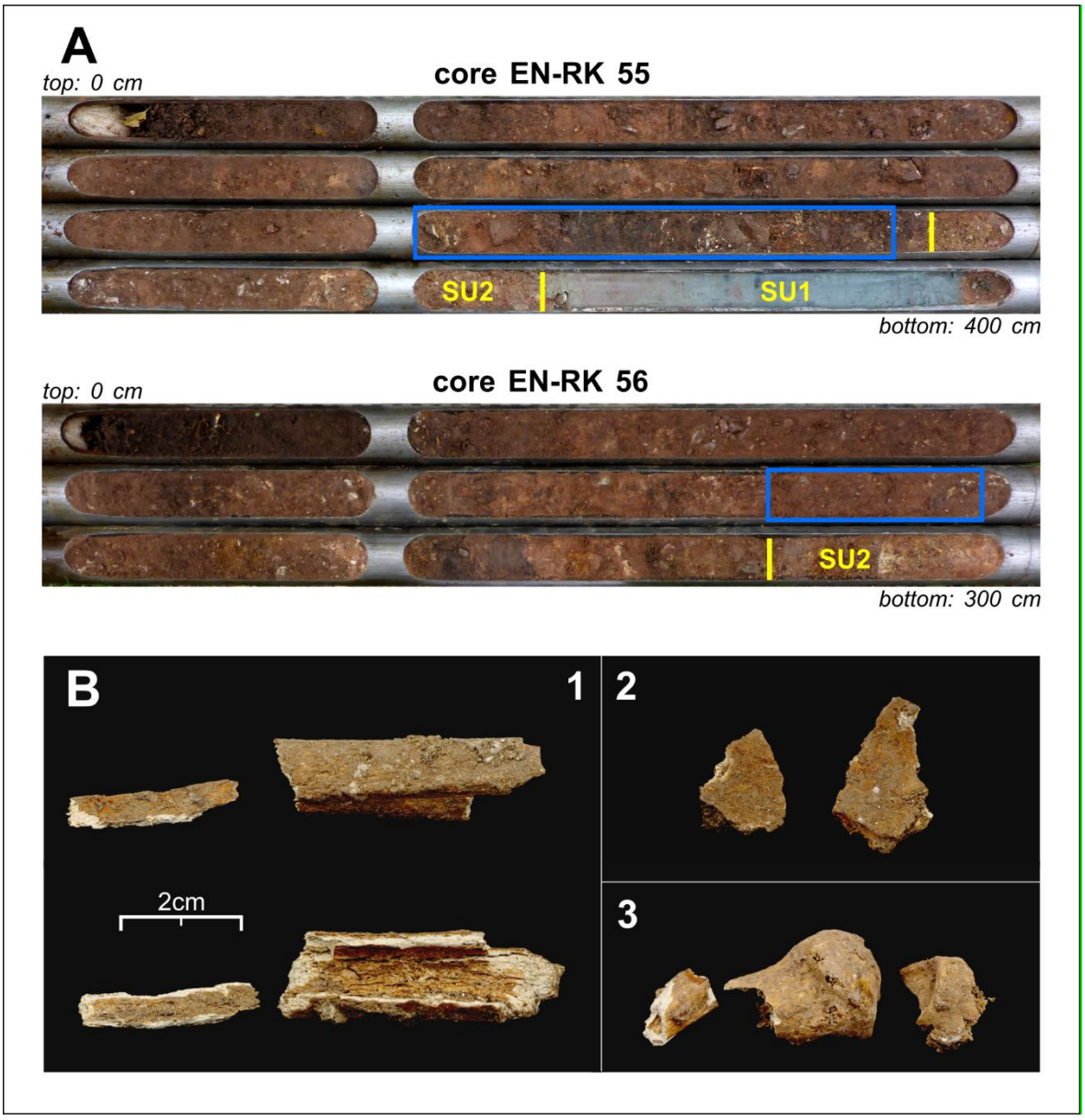

***Fig. 7: A** – Photographic documentation of the core EN-RK 55 and 56 within the potential mass grave. SU1 refers to the Keuper mudstone, SU2 to Lower Terrace fluvial gravels. The backfill deposits comprise the entire sequence above the boundary with SU2. Blue boxes indicate the main occurrence of well-preserved skeletal remains. **B1** – Fragments of a longbone from EN-RK 55 (264 cm depth), **B2** – Fragments of cranial bones from EN-RK 55 (260 cm depth), **B3** – Bone fragments from EN-RK 56 (180 cm depth).*

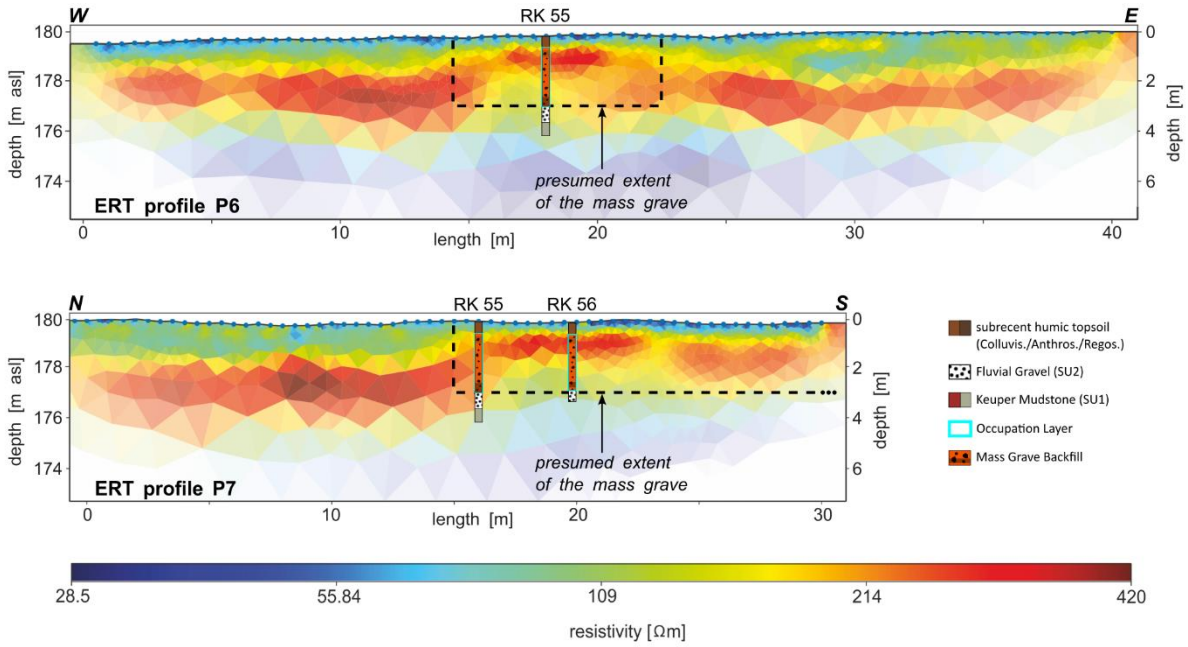

***Fig. 8**: ERT-profiles P6 and P7 (electrode spacing of 0.5 m, model is based on a joint inversion of a Wenner and Dipole-Dipole configuration), crossing the potential mass grave in a W-E, resp. N-S direction. The vertical and horizontal extent of the potential mass grave based on concurring findings of ERT and Pürckhauer mapping is indicated with black dashed lines.*

In the respective cores EN-RK 55 and 56, which are about three meters apart (Fig. 3), the natural stratification is substantially disturbed down to even greater depths (approx. 280 cm) than was evidenced by the shallow (1 m) Pürckhauer soundings. An intricate mixing of all natural deposits (SU2 to SU5) from these upper ~3 m with varying degrees of uniformity leads to anomalous contents of organic matter and the clastic coarse-grained fraction throughout the backfill sequences (Fig. 7A). The lower boundary of the anomalous feature is formed by the contact with the gravels of SU2, situated at 285cm (EN-RK 55) and 270cm (EN-RK 56). But in fact, since stones and pebbles, stemming from SU2 are dispersed across the disturbed part of the sequence, this boundary needs to be regarded as artificially lowered down during the historical excavation process. Accordingly, in core EN-RK 55, the original SU2 gravels below the feature have only about a third of their usual thickness (ca. 60cm) (Fig. 7A). Apart from allochthonous coarse-grained material, the sediment matrix contains small lumps (<1cm) of seemingly unaltered primary loess (SU5.1) throughout the disturbed segments. And it overall shows higher silt and fine sand contents than would be usual for SU3 at comparable depths outside of the anomaly. This testifies to the admixture of loess into the backfill deposits, which in turn means that

the entire structure originates from a time before the large-scale removal of the loess in this part of the AOI in 1926/27. Among the unusual constituents found in the backfill are also clearly anthropogenic ones: dispersed brick fragments, charcoal pieces and human skeletal remains. The latter mainly occur between 235 and 280 cm in EN-RK 55, where they also coincide with the most humic deposits, and in EN-RK 56 between 170 and 190 cm coring depth (Fig. 7).

In the ERT profiles, the anomaly is reflected by a thinning of the low-resistivity capping deposits and an updoming of the high-resistivity segments below, likely due to the admixture of coarser grain sizes. In P6, the feature is located approximately in the middle of the profile, while it starts at around 15m profile length in P7 (Fig. 8). The lower boundary of the backfill, however, is nearly invisible in ERT. Instead, high resistivity values of the updomed coarse-grained deposits (>200 Ωm) slowly grade downwards into the low values (<70 Ωm) of the underlying Keuper mudstone (SU1).

Based on the Pürckhauer prospection and the ERT result, we tentatively delimit the anomalous feature as follows (Fig. 8): In W-E orientation, a length of ~9 meters is implied, with core EN-RK 55 positioned right at the center. In N-S orientation, the northern margin is just one meter north of EN-RK 55, both in ERT and according to Pürckhauer prospection. Locating the southern margin was hampered by an impenetrable blackthorn (*Prunus spinosa*) thicket, but the total length was confirmed to be more than 15 meters.

3.3 Chronology

The pottery sherds and charcoal pieces sampled from occupation layers and archeological features during the coring campaign can provide first chronological orientation and might reflect the settlement period of the former village Neuses. For three charcoals from cores EN-RK 21, 53 and 55, calibrated radiocarbon ages ranging from the 11th to the 13th century were obtained, whereas one from the lower part of the potential mass grave backfill in EN-RK 56 at 243 cm gave an Early Neolithic age (Tab. 2). Out of the fourteen pottery sherds, seven pieces collected from cores EN-RK 27, 32, 38, 47 and 48 could be classified as (tentatively) medieval (Tab. 2, Fig. 9). The two bone fragments taken from the cores EN-

RK 55 and 56 within the potential mass grave showed optimal collagen preservation (C/N values of 3.2, collagen contents of 4.4% and 7.3%), and they returned virtually identical age ranges with 1302-1401 and 1301-1398 cal AD (2σ) (Tab. 2). A higher dating accuracy was hampered by strong fluctuations of the radiocarbon calibration curve for this period (68). Further methodological details on the dating approaches can be found in Supplementary Section 5.1.

***Tab. 2**: Compilation and sampling context of different chronological information from the study area. Abbreviations for pottery: PH=Prehistory, MA=Middle Ages, LMA=Late Middle Ages, MO=Modern era. *For this sample, the cal BC scale applies, instead of cal AD. For pottery finds, the inventory number of the Thuringian State Office for Monument Preservation and Archaeology is indicated in italics. For radiocarbon samples, we state the MAMS laboratory code from CEZA in Mannheim (bold).*

Core EN-…	Depth [cm]	*Lab code*/ **Inv. No.**	Layer	Pottery	^{14}C Bone cal AD (2σ)	^{14}C Charcoal cal AD (2σ)
RK 21	130	*60284*	occupation layer/feature	-	-	1169-1265
RK 32	45	**22/220-4**	overbank deposit/occ. layer?	PH-MA	-	-
RK 32	85	**22/220-7**	overbank deposit/occ. layer?	PH	-	-
RK 35	80	**22/220-10**	overbank deposit/occ. layer	PH	-	-
RK 38	36	**22/220-1a**	colluvial deposit/occ. layer	MA/MO	-	-
RK 38	36	**22/220-1b**	colluvial deposit/occ. layer	MO	-	-
RK 46	53	**22/220-2**	overbank deposit (BFS)	PH	-	-
RK 47	41	**22/220-6**	overbank deposit (BFS)	MA	-	-
RK 48	38	**22/220-5a**	occupation layer/feature	MA	-	-
RK 48	38	**22/220-5b**	occupation layer/feature	PH-MA	-	-
RK 48	55	**22/220-8**	occupation layer/feature	MA	-	-
RK 53	40	*60282*	topsoil, truncated occ. layer	-	-	1035-1160
RK 57	45	**22/220-11a**	topsoil/occ. layer	PH	-	-
RK 57	45	**22/220-11b**	topsoil/occ. layer	MO	-	-
RK 55	154	*60281*	feature, possible mass grave	-	-	1038-1204
RK 55	260	*60280*/ **22/220-13**	feature, possible mass grave	-	1302-1401	-
RK 56	180	*65026*/ **22/220-20**	feature, possible mass grave	-	1301-1398	-
RK 56	243	*65027*	feature, possible mass grave	-	-	4447-4337*****

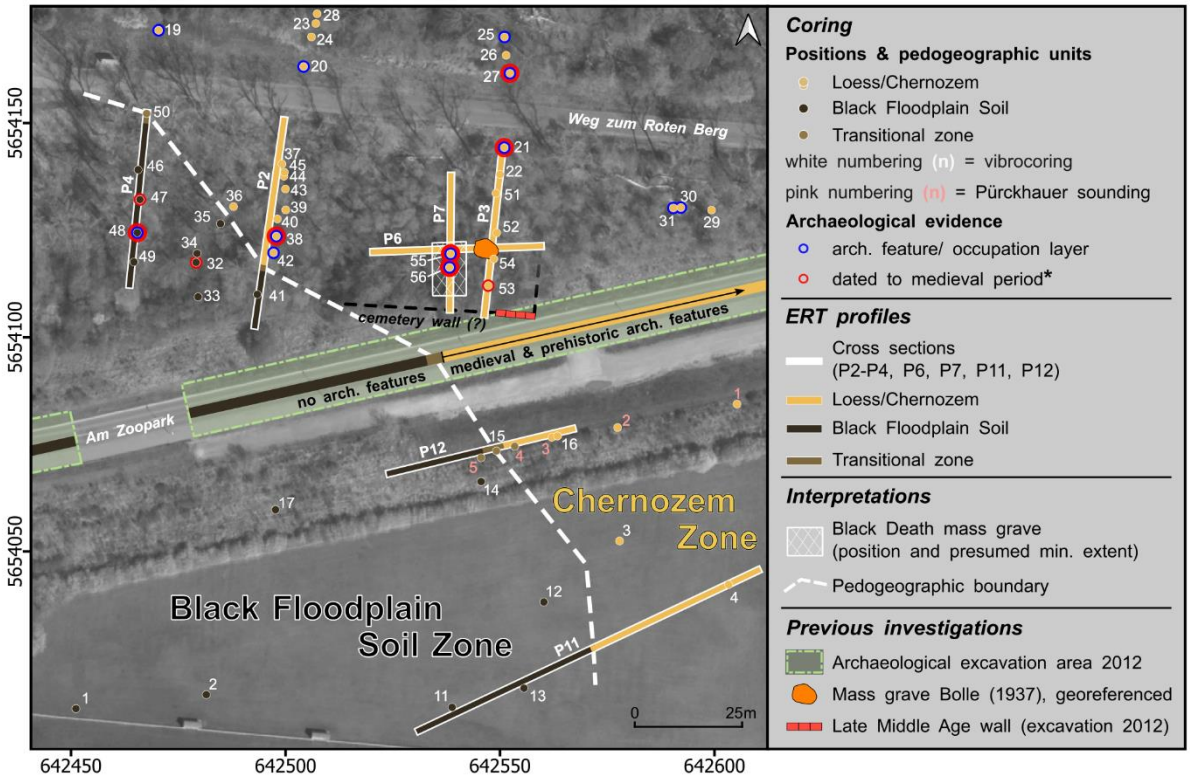

Fig. 9: *Synoptic illustration of the main results, integrating ERT and coring to infer the regionalization of the pedo-lithostratigraphic zones, with their boundary indicated as a white dashed line. Coring positions with presumed archaeological subsurface features are marked in blue, positions with available chronological information are (additionally) marked in red. Findings of previous archaeological investigations are indicated, as is the presumed position of the former cemetery wall (Supplementary Section 5.2) and extent of the mass grave, discovered in this study. *For details regarding the chronologies, see Tab.2.*

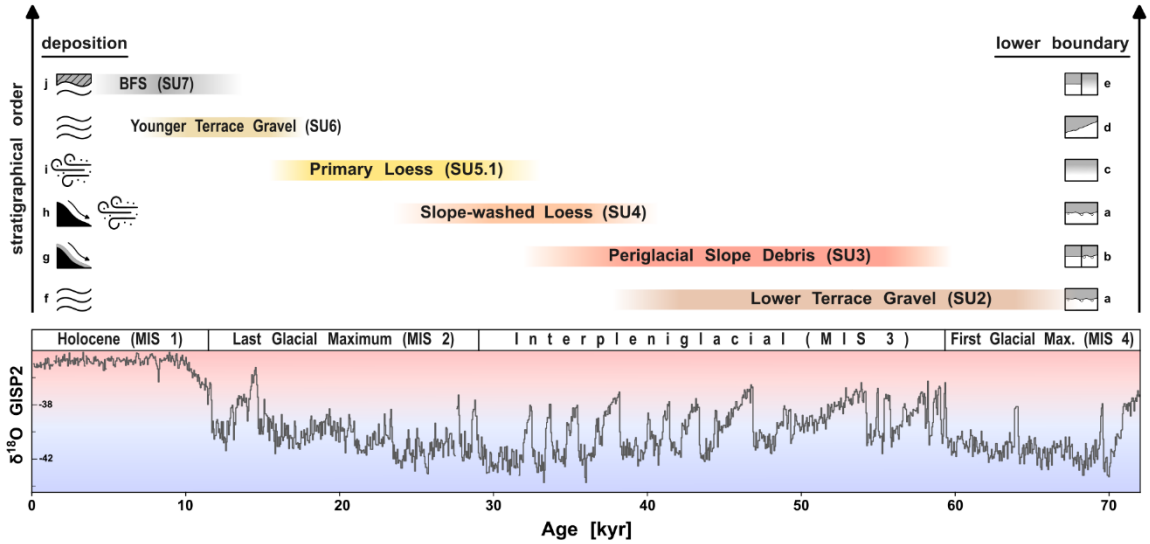

Fig. 10: *Neuses fluvio- and hillscape evolution model. Preliminary chronostratigraphy of all natural deposits encountered in the study area, see also the explanation in the text. Letters a-e (right) denote the characteristic of the respective lower boundary: **a** – erosionally disconform, **b** – (erosionally) disconform, **c** – gradual, **d** – laterally-erosional disconform, **e** – gradual to disconform. Letters f-k (left) relate to the main depositional process: **f** – fluvial, **g** – solifluctive, **h** – colluvial and aeolian, **i** – aeolian, **j** – alluvial (overbank deposition). GISP2 $\delta^{18}O$ ice core record and the MIS boundaries for temporal and palaeoclimatic reference (Lisiecki and Raymo, 2005; Rasmussen et al., 2014).*

4. Discussion

4.1 Implications for landscape evolution

Despite sparse numerical age control for the sedimentological deposits, relative stratigraphies and pedosedimentary characteristics allow to propose a first and tentative Neuses fluvio- and hillscape evolution model (Fig. 10):

1. After the deposition of the Upper Middle Terrace in the late Elsterian on top of the Keuper remnant "Roter Berg" (48), multi-phased valley formation took place over the course of the Saalian and Early Weichselian, preferentially during climatic transitions (72). This incision eventually exposed the Keuper Mudstones (SU1) at the slopes of the "Roter Berg".

2. The erosional surface became covered by the gravels of the upper Pleistocene Lower Terrace (SU2) in due course. In Thuringia, this terrace formation is assigned to the Weichselian Pleniglacial (48). In the (wider) region, well-dated fluvial archives place the most intense pleniglacial fluvial activity and aggradation into MIS 4 and 3, again mainly controlled by climatic transitions (73–77).

3. Thereafter, slope deposition became the dominant process in the "Roter Berg" area, comprising Stratigraphic Units SU3 and SU4. This is a clear indication for a destabilizing but still rather humid landscape, for which a lot of evidence exists in Central Europe from ca. 40-45 ka (later Interpleniglacial/MIS 3) onwards, when a general cooling tendency can be observed (78–80). We consider SU3 to be a polygenetic periglacial slope debris that formed with the participation of (i) mass wasting/active layer failure, preserving the original structure of reworked SU1, (ii) solifluction events that homogenized weathered gravels from the Upper Middle Terrace, Keuper Mudstone and early loess, creating massive and very poorly-sorted sediments, and (iii) slope-wash processes making for well-sorted interbeds of loess-like deposits. All of these processes and combinations thereof are well-known to have occurred in Central European mudstone landscapes during the Weichselian Pleniglacial (81–83). The laminated slope-washed loess (SU4) overlies SU3 following another erosional disconformity, implied by the accumulation of residual gravel directly at their boundary. Such deposits are documented in loess sections

across Central and Western Europe, where they often represent slowly aridifying landscapes around the MIS 3/2 boundary with accelerating loess deposition (84–86).

4. As the laminated slope-washed loess of SU4 grades into the massive primary loess of SU5.1, a continuing aridification and cooling trend leading to increased aeolian activity can be inferred. Both, in Central Europe and also specifically in Central Germany, the driest phase of the Weichselian and the main loess delivery phase occurred between ca. 25 and 17 ka (78,84,85,87–89). It therefore seems reasonable to assign the deposition of SU5.1 to this period.

5. In the aftermath of loess deposition, in the southwestern part of the study area, another fluvial activity phase is evident, that extensively cleared out SU2 to SU5.1 beyond a sharp lateral contact. In their stead, a fluvial terrace fill (SU6) was deposited unconformably on SU1. While SU6 is situated in the area of Lower Terrace deposits according to the geological map (Fig. 1), it can be differentiated from the older SU2 by its carbonate and gravel content, its petrography, sedimentary structure with indications of fining-up segments, and by its higher relative elevation (Fig. 6; SI Fig. 4; Supplementary Section 3.2). The stratigraphic position and these characteristics might qualify SU6 as a latest Weichselian to Early Holocene gravel, when fluvial architectures gradually changed from a braided to a single-channel meandering style. In fact, a lot of indications from different Central European fluvial catchments point to the Weichselian/Holocene boundary for the youngest stages of Lower Terrace formation (75–77,82,90,91). Hence, a correlation of SU6 with this transitional phase appears plausible.

6. Within the primary loess of SU5.1, a Chernozem (SU5.2) formed. While the preconditions for its pedogenesis and preservation are still somewhat controversial, dry climatic conditions, carbonate availability in the solum, specific bioturbation modes and the (possibly anthropogenic) admixture of charred organic matter (black carbon) seem to play the most important roles (92–96). For Central Germany, a formation time from the Weichselian Lateglacial/Early Holocene to about 6 or 5 ka BP is assumed (92,97). Subsequently, local to regional decalcification has apparently led to a complex spatial pattern of degradation towards (luvic) Phaeozems and Luvisols (94,98). It is noteworthy that

(haplic/calcic) Chernozems and subordinately also decalcified (luvic) Phaezems occur in our study area in very close proximity. Hence, we cautiously attribute the patchy Chernozem degradation here to locally variable occupation and land-use impact on these agronomically important soils since the Early Neolithic (cf. 99).

On top of SU6, a Black Floodplain Soil (SU7) was formed and/or deposited in the Gera floodplain and still remains largely uncovered at the surface of our study area today. The same has been documented in the Rhine, Main and Weser River catchments in Germany, where similarly thick, clayey-humic fluvisols (labelled as "Pseudochernozems") developed on calcareous gravels of the latest Weichselian and earliest Holocene fluvial terraces in the Alleröd and Preboreal, respectively (100,101). Apart from that, Black Floodplain Soils are typically buried under thick sequences of clastic overbank deposits (102). They are characterized by >30cm of a clayey and highly-humic solum, formed either (i) by selective erosion of clay-humus complexes from surrounding Chernozem plateaus, (ii) decomposition of *in-situ* organic matter or (iii) as gyttjas under water-logging conditions. Estimated ages for Black Floodplain Soil formation usually range from the Early Holocene to the Atlantic period (102–106). On a more regional scale, since for the Black Floodplain Soil zone in the study area the toponym "Rieth-Feld" is used ("reed field") (SI Fig. 1A), a connection to the eponymous geological "Rieth"-series in Thuringia could likely be drawn. This sequence of peat and organic mud deposits is generally assigned to the Early Holocene (48). Based on these references, it seems appropriate to assume a mainly Early to Mid-Holocene formation/deposition of the Black Floodplain Soil within the study area.

4.2 Historical and archeological implications

4.2.1 Successful (re)discovery of a Black Death mass grave?

The anomalous subsurface feature that we detected contains human skeletal remains in different depths and segments (SI Tab. 2, Supplementary Section 5.3). Two bones from the cores EN-RK 55 and 56 were subjected to radiocarbon dating. As the cores are about three meters apart, it can likely be

ruled out, that the same specimen was accidentally sampled twice between the cores. Therefore, the nearly identical dating results (1302-1401 and 1301-1398 cal AD) (Tab. 2) on the two bones not only strengthen the overall chronology, but also testify to a contemporaneous interment of several individuals in the 14th century. The anomaly has the considerable horizontal extent of 9 by >15 meters and we reconstructed a depth of ~3.5 meters from the coring depth of ~2.8 meters and at least 0.7 meters of soil removal for the airfield construction in 1926/27 (Fig. 5). This results in >470 m³ or about 750 t of material when assuming a cuboid shape and a bulk density of 1.6 g/cm^3. Taking together these findings, the most plausible interpretation of the anomaly is indeed that of a mass grave (107). If there was no further historical context, the designation as a Black Death pit would, however, still be premature, even with the chronology established. Alternative reasons for the construction of a mass grave, i.e. alternative causes of mass fatalities in that time span comprise climatic disasters, conflicts, famine or other illnesses (32,33). Fortunately in the case of Neuses, contemporary written sources are very specific on the timing (July 1350 to February 1351), location (cemetery of Neuses) and high number of the burials (12000 bodies in 11 pits) connected with the Black Death outbreak (46). Since most of the documentation and all the skeletal finds from the 1926/27 excavation have been lost, the results of our investigations can now (i) not only independently confirm the presence of a mass grave in a very similar position, but (ii) can also chronologically attribute the timing of the burials to the 14th century for the first time. Whether the mass grave that we exposed through vibracoring and ERT is indeed identical with the one previously discovered cannot be resolved, nor is it strictly relevant. Most significantly, and unique in comparison to all other Black Death mass graves, our prospection findings and the dating of the human bones (within the confines of uncertainty) are absolutely consistent with the detailed historical accounts. Therefore, we are confident of the successful (re)discovery of at least one of the Black Death mass graves in the Erfurt region. Its expected dimensions are far above the average of contemporaneous ones in Europe, so that according to our knowledge only the burials in Thornton Abbey (GB) compare in their extents, if not depths (21). In Neuses, further exploration for the

remaining ten specified plague pits has the unique potential to directly assess the validity of the written sources also regarding the specific number of those pits and buried bodies.

4.2.2 Natural setting, village and mass grave – spatio-temporal relationships

According to Bolle (45,54), the church of Neuses has been built in the 12th century, while he places the foundation of the village a bit earlier, before 1100 AD. This is in agreement with our few ^{14}C-dated charcoals, sampled from occupation layers across the AOI, and the age determination of the pottery sherds (Tab. 2, Fig. 9). While evidence for activity in the High and Late Middle Ages is present in our data, clear indication for Early Medieval activity is lacking so far. The position and spatial organization of the former village seem to be inextricably linked with the juxtaposition of the two pedogeographic zones in the AOI and their extents (Fig. 9). Considering the findings of the two excavations in 1926/27 and especially in 2012, all the archeological features and structures that could be related to Neuses are situated within the Chernozem zone, whereas only a few single finds have been made in the Black Floodplain Soil zone (45,55,108). Up until the mid-19th century, wetlands stretched in the area south of “Roter Berg”, where in places, peat was cut and stagnant water surfaces existed (Kirchhoff, 1895; Lehmann, 1928). Correspondingly, Neuses was situated entirely on the higher and drier ground of the loess area with fertile chernozem soils but on the margins of the wetter lowlands extending in the distal River Gera floodplain. A valley edge position of the former village had already been concluded by Bolle (45) and implicitly by Sczech (55), and it can now be substantiated and localized based on our findings. The evidence suggests that the former village of Neuses was aligned, both, with the “Weg zum Roten Berg” as seen for the orientation of the former cemetery wall (Fig. 9, Supplementary Section 5.2), and with the natural situation, i.e., with the margin towards the Black Floodplain Soil zone. According to our results, not only the village itself, but also the regular cemetery and the Black Death mass graves were located in the Chernozem zone. This seems to imply a certain awareness that the former wetland area of the Black Floodplain Soil zone would have provided much less favorable soil conditions for the decomposition of the bodies in single burials and especially mass graves – a fact

which is well-known today and taken into account for the planning of regular and emergency burials alike (110,111).

The timing of the village's demise and abandonment cannot be easily determined on the basis of historical documents (45). In 1354, Neuses was last referred to as ‘villa’ (village) in written sources, while in 1516 it was described as “long-since abandoned”, whereas the church was still standing until the end of the 17th century. Bolle (45) postulates that it was most likely deserted between 1354 and the middle of the 15th century. Our own chronological information on that matter is sparse, but the dates for the occupation period seem to cluster in the High to Late Middle Ages with no clear indication for activity in the 15th century and beyond (Tab. 2). Largely the same can be said for the preliminary age determinations during the 2012 excavation (55,108). Bolle’s assessment can therefore be broadly confirmed by the chronological data obtained recently, even if a more precise time frame of the event is still not established.

Maybe the general choice of burial location for the Black Death casualties of Erfurt might be an additional clue as to when the desertion process occurred for Neuses. The question arises: Why was Neuses chosen of all places? It stands to reason, that by deliberation, consecrated ground in nearby villages was preferred for the emergency interments in order to at least partially adhere to Christian burial conventions (112,113). But given the urgency of the situation and the diminishing capacity of available work force, it does seem peculiar that the choice fell on Neuses, about 5 km away from the city, rather than a more proximal village. Hence, other explanations need to be considered besides logistics, such as the notion that Neuses had already been deserting or even deserted by 1350, thus leaving available space on the cemetery. Additionally, of course also political and legal aspects preconditioned the choice of Neuses as a burial site. Most importantly, we know from written sources that Erfurt’s city council held the patronage rights for the parish church of Neuses (54) and that the council was advised by medical scholars to dispose of the dead in specially-excavated ditches (46) which apparently could only be realized on grounds under the council’s control. In the future, we hope to shed more light on

the site selection and a potential relation to the desertion of the village, *inter alia* with a thorough analysis of the 2012 archeological excavation data along with continuing studies of the written sources.

4.3 Assessment of the combined prospection approach

For the identification and investigation of the Black Death mass grave in Erfurt, we loosely followed well-established procedures, primarily developed for war crime burials (33,43,114), but also widely used in archeology (34,36,115). We successfully narrowed down the potential burial site with a desk study of historical and available archeological documentation (20,45,52,54,55) as well as remote sensing data.

In the target area, we conducted combined non-invasive geophysical and minimally-invasive coring surveys for stratigraphic and pedogenic reconnaissance. The coupling of different geophysical techniques is generally considered best practice for a successful detection of mass graves (43,116), while GPR is regularly reported to produce more meaningful results than ERT (34,36,37,117–119). In our case, the opposite effect has occurred. The GPR signal fell short as it apparently attenuated in contact with the thick and fine-grained cover layers of loessic deposits and loamy slope debris (SU3 to SU5), so that no expressive data could be obtained (61,117). Conversely, our ERT data in conjunction with the spatially well-resolved borehole information yielded valuable insights into the near-surface natural deposits, also clearly resolving stratigraphic boundaries based on grain-size differences. Similar conclusions were drawn from geomorphological investigations of equally fine-grained floodplain deposits contrasting with underlying fluvial gravels (120,121). Thus, ERT both confirms and complements our vibracoring findings, especially regarding the position of the pedogeographic boundary between the Chernozem and Black Floodplain Soil zones (Fig. 9, Supplementary Sections 3 and 4).

An additional important outcome of the reconnaissance phase are our estimates for the amount of soil removal due to ground levelling in 1926/27 in the suspect area for the mass grave: ~100 cm in transect T2 and ~70 cm in T3. Those numbers are derived from lacking and/or truncated stratigraphic units SU4 and SU5 (Fig. 5) and are the prerequisites for assessing the original depth of the mass grave

at the time of its layout. In the next phase of our fieldwork, a systematic survey for the mass grave could be conducted, facilitated by stratigraphic background knowledge and the prior mutual "calibration" of borehole and ERT results. The lack of these two aspects has previously been identified as a main cause for low detection success of burial features in other studies, where the ERT anomalous signal was masked by (unknown) naturally heterogeneous depositional settings (e.g. 119). Even so, geomorphological or landscape-oriented off-site investigations are only rarely applied as a supplement of geophysics to increase the recognition of such features (115,but see 122). For Neuses, not least because of the combination with independent coring data, ERT proved a well-suited geophysical method for the detection of the mass grave and characterization of the natural background alike. Final identification of the mass grave anomaly was enabled by the fact that the original dig in 1350/51 cut into the topmost fluvial gravels (SU2) which were then redeposited further up in the shaft together with the more fine-grained backfill originating from SU3 to SU5. The unusual presence of these sporadic gravels at shallow depths both raised initial suspicions throughout the Pürckhauer soundings and caused an ERT-sensitive highly resistive disturbance contrasting with the surrounding sediment matrix (21,cf. 43). Apart from the effective localization of the mass grave and its subsequent chronological assignment to the 14th century, a 3D delimitation could also be established. In this regard, once again, the respective strengths of vibracoring and ERT complemented one another. Whereas the lower boundary of the grave anomaly was near-invisible in the ERT profiles, it could readily be detected in the cores EN-RK 55 and 56 (Figs. 7, 8). Vice versa, compared to vibracoring, ERT provided a much more time-efficient way to trace the horizontal extents of the mass grave (profiles P6 and P7), even though the exact shape and the southern margin could not be recorded so far.

Methodologically, the surveys in Neuses demonstrated the applicability of combined ERT and vibracoring techniques to detect and delineate mass graves in challenging settings. In our case, dense vegetation impeded the use of 3D geophysical methods such as EMI and moreover, former large-scale ground modifications have significantly compromised the natural depositional situation in the target area. These challenges could be bypassed by an extensive stratigraphic exploration of the surrounding area

in close mutual consultation of ERT and sediment coring, fostering the identification of slight deviations from natural standards. Our interpretations and the mentioned challenges may be unique to our site, but our method combination holds the potential to successfully resolve the mapping of similarly demanding sites for archeological and forensic investigations (38,123,124).

5. Conclusion

The outbreak of the Black Death in Erfurt and the putative mass grave situated outside its city walls in the village of Neuses are unique on a European scale: Dense historical accounts together with initial 20th century archeological findings allow for the first ever systematic survey of a mass grave related to the second plague pandemic. Building on the existing data, our main objective was to detect a mass grave in Neuses so that material for dating and later genetic studies could be gained. To that end, we chose a prospection approach with a close coupling of electrical resistivity tomography and vibracoring. The results helped unravel the natural stratigraphic situation, which could vertically be subdivided into seven stratigraphic units, while spatially, two distinct pedogeographic areas could be identified: a Chernozem zone and a Black Floodplain Soil zone, the latter still being wetlands in medieval times. As these wetlands apparently remained unoccupied back then, this information also provided valuable insights into the positioning and internal organization of the former village and cemetery. The discovery of the mass grave was decisively facilitated by the obtained pedostratigraphic knowledge, which helped to better recognize slight deviations against the natural background. Two human bones from the mass grave structure were AMS radiocarbon dated to the 14th century, reinforcing the assumption that the previously and recently found mass graves can indeed be related to the Black Death.

To our knowledge, our research represents the first instance where an unmarked Black Death mass grave was found through systematic prospection. It offers a rationale to support the widely-used geophysical methods with an extensive independent stratigraphic survey, especially in similarly

demanding settings, where e.g., dense vegetation and strong ground modifications might otherwise hamper the detectability.

Author contributions

MH: conceptualization, writing–original draft, investigation, visualization, data curation, methodology. **NU:** conceptualization, investigation, writing–review and editing. **AE:** investigation, methodology, writing–original draft. **JRV:** conceptualization, writing–review and editing, visualization, data curation. **JS:** conceptualization, writing–review and editing. **MS:** investigation, formal analysis, methodology, visualization. **MP:** investigation, methodology, formal analysis, data curation. **IN:** investigation, methodology, writing–original draft, writing–review and editing. **MO:** methodology, visualization, writing–review and editing. **LW:** conceptualization, writing–review and editing. **BS:** data curation, methodology, writing–review and editing. **CT:** data curation, methodology, writing–review and editing. **AH:** conceptualization, writing–review and editing. **JN:** conceptualization, writing–review and editing. **UW:** funding acquisition, conceptualization, investigation, methodology, data curation, validation, writing–original draft. **MB:** funding acquisition, conceptualization, investigation, methodology, data curation, writing–original draft, writing–review and editing. **CZ:** funding acquisition, conceptualization, investigation, writing–original draft, writing–review and editing.

Acknowledgements

We are grateful to Susanne Lindauer, *Curt-Engelhorn-Zentrum Archäometrie GmbH* (CEZA) in Mannheim for carrying out radiocarbon dating, to the City of Erfurt and family Dittmar for granting access to their properties, and to *Schollenberger Kampfmittelbergung GmbH* for conducting the exploration for explosive ordnance prior to our investigations. We would further like to express out thanks to Peter Jung and the geography students of Leipzig University (course 12-GGR-B-PG05, summer term of 2023) for actively supporting fieldwork and for asking all the right questions.

References

1. Aberth J. The Black Death: a new history of the great mortality in Europe, 1347-1500. New York (N.Y.): Oxford (GB) Oxford University Press; 2021.

2. Benedictow OJ. The Complete History of the Black Death [Internet]. Boydell & Brewer; 2020 [cited 2023 Sep 4]. 1200 p. Available from: http://www.jstor.org/stable/10.2307/j.ctvxhrjg8

3. Izdebski A, Guzowski P, Poniat R, Masci L, Palli J, Vignola C, et al. Palaeoecological data indicates land-use changes across Europe linked to spatial heterogeneity in mortality during the Black Death pandemic. Nat Ecol Evol [Internet]. 2022 Feb 10 [cited 2023 Sep 4];6(3):297–306. Available from: https://www.nature.com/articles/s41559-021-01652-4

4. Ben Ari T, Neerinckx S, Gage KL, Kreppel K, Laudisoit A, Leirs H, et al. Plague and Climate: Scales Matter. Manchester M, editor. PLoS Pathog [Internet]. 2011 Sep 15 [cited 2023 Sep 4];7(9):e1002160. Available from: https://dx.plos.org/10.1371/journal.ppat.1002160

5. Bos KI, Schuenemann VJ, Golding GB, Burbano HA, Waglechner N, Coombes BK, et al. A draft genome of Yersinia pestis from victims of the Black Death. Nature [Internet]. 2011 Oct 27 [cited 2023 Sep 4];478(7370):506–10. Available from: https://www.nature.com/articles/nature10549

6. Slavin P. The Birth of the Black Death: Biology, Climate, Environment, and the Beginnings of the Second Plague Pandemic in Early Fourteenth-Century Central Asia. Environ Hist [Internet]. 2023 Apr 1 [cited 2024 Aug 24];28(2):300–34. Available from: https://www.journals.uchicago.edu/doi/10.1086/723955

7. Spyrou MA, Musralina L, Gnecchi Ruscone GA, Kocher A, Borbone PG, Khartanovich VI, et al. The source of the Black Death in fourteenth-century central Eurasia. Nature [Internet]. 2022 Jun 23 [cited 2023 Sep 4];606(7915):718–24. Available from: https://www.nature.com/articles/s41586-022-04800-3

8. Barker H. Laying the Corpses to Rest: Grain, Embargoes, and *Yersinia pestis* in the Black Sea, 1346–48. Speculum [Internet]. 2021 Jan 1 [cited 2023 Sep 4];96(1):97–126. Available from: https://www.journals.uchicago.edu/doi/10.1086/711596

9. Green MH. The Four Black Deaths. Am Hist Rev [Internet]. 2020 Dec 29 [cited 2023 Sep 4];125(5):1601–31. Available from: https://academic.oup.com/ahr/article/125/5/1601/6040962

10. Slavin P. From the Tian Shan to Crimea: Dynamics of Plague Spread during the Early Stages of the Black Death, 1338–46. J Econ Soc Hist Orient [Internet]. 2023 Jun 7 [cited 2024 Aug 24];66(5–6):513–627. Available from: https://brill.com/view/journals/jesh/66/5-6/article-p513_1.xml

11. Schmid BV, Büntgen U, Easterday WR, Ginzler C, Walløe L, Bramanti B, et al. Climate-driven introduction of the Black Death and successive plague reintroductions into Europe. Proc Natl Acad Sci [Internet]. 2015 Mar 10 [cited 2023 Sep 4];112(10):3020–5. Available from: https://pnas.org/doi/full/10.1073/pnas.1412887112

12. Belich J. The World the Plague Made: The Black Death and the Rise of Europe [Internet]. Princeton University Press; 2022 [cited 2024 Aug 24]. Available from: http://www.jstor.org/stable/10.2307/j.ctv287skgm

13. Ljungqvist FC, Tegel W, Krusic PJ, Seim A, Gschwind FM, Haneca K, et al. Linking European building activity with plague history. J Archaeol Sci [Internet]. 2018 Oct [cited 2023 Sep 22];98:81–92. Available from: https://linkinghub.elsevier.com/retrieve/pii/S0305440318302693

14. Bos KI, Herbig A, Sahl J, Waglechner N, Fourment M, Forrest SA, et al. Eighteenth century Yersinia pestis genomes reveal the long-term persistence of an historical plague focus. eLife [Internet]. 2016 Jan 21 [cited 2023 Sep 22];5:e12994. Available from: https://elifesciences.org/articles/12994

15. Namouchi A, Guellil M, Kersten O, Hänsch S, Ottoni C, Schmid BV, et al. Integrative approach using *Yersinia pestis* genomes to revisit the historical landscape of plague during the Medieval Period. Proc Natl Acad Sci [Internet]. 2018 Dec 11 [cited 2023 Sep 22];115(50). Available from: https://pnas.org/doi/full/10.1073/pnas.1812865115

16. Spyrou MA, Keller M, Tukhbatova RI, Scheib CL, Nelson EA, Andrades Valtueña A, et al. Phylogeography of the second plague pandemic revealed through analysis of historical Yersinia pestis genomes. Nat Commun [Internet]. 2019 Oct 2 [cited 2023 Sep 4];10(1):4470. Available from: https://www.nature.com/articles/s41467-019-12154-0

17. Slavin P. Out of the West: Formation of a Permanent Plague Reservoir in South-Central Germany (1349–1356) and its Implications. Past Present [Internet]. 2021 Aug 4 [cited 2023 Sep 4];252(1):3–51. Available from: https://academic.oup.com/past/article/252/1/3/6120066

18. Carmichael AG. Plague Persistence in Western Europe: A Hypothesis. Mediev Globe [Internet]. 2015 [cited 2024 Aug 24];1(1):157–91. Available from: https://muse.jhu.edu/article/758488

19. Parker CE, Hiss AN, Spyrou MA, Neumann GU, Slavin P, Nelson EA, et al. 14th century Yersinia pestis genomes support emergence of pestis secunda within Europe. Falush D, editor. PLOS Pathog [Internet]. 2023 Jul 18 [cited 2023 Sep 4];19(7):e1011404. Available from: https://dx.plos.org/10.1371/journal.ppat.1011404

20. Bauch M, Oertel C. Late Medieval Plague Waves in in Eastern Germany and Bohemia: Combining Narrative, Administrative, Epigraphic and Pictorial Sources with Quantitative Approaches. Hist Stud Cent Eur [Internet]. 2024 Jul 24 [cited 2024 Aug 24];4(1):30–67. Available from: https://ojs.elte.hu/hsce/article/view/8092

21. Willmott H, Townend P, Swales DM, Poinar H, Eaton K, Klunk J. A Black Death mass grave at Thornton Abbey: the discovery and examination of a fourteenth-century rural catastrophe. Antiquity [Internet]. 2020 Feb [cited 2023 Sep 4];94(373):179–96. Available from: https://www.cambridge.org/core/product/identifier/S0003598X19002138/type/journal_article

22. Bauch, M., Wozniak, T. Mass Grave. In: EpiMedDat [Internet]. Available from: http://epimeddat.net/index.php?title=Mass_grave

23. Castex D, Kacki S. 'Bring Out Your Dead.' In: The Routledge Handbook of Archaeothanatology [Internet]. 1st ed. London: Routledge; 2022 [cited 2024 Aug 25]. p. 331–52. Available from: https://www.taylorfrancis.com/books/9781351030625/chapters/10.4324/9781351030625-21

24. Franklin ER, Mitchell PD, Robb J. The Black Death in Hereford, England: A demographic analysis of the Cathedral 14th-century plague mass graves and associated parish cemetery. Am J Biol Anthropol [Internet]. 2023 Aug 31 [cited 2023 Sep 22];ajpa.24838. Available from: https://onlinelibrary.wiley.com/doi/10.1002/ajpa.24838

25. Grainger I, Hawkins, Duncan, Cowal, Lynne, Mikulski, Richard. The Black Death cemetery, East Smithfield, London. London: Museum of London Archaeology Service; 2008. 63 p. (MoLAS monograph).

26. Haensch S, Bianucci R, Signoli M, Rajerison M, Schultz M, Kacki S, et al. Distinct Clones of Yersinia pestis Caused the Black Death. Besansky NJ, editor. PLoS Pathog [Internet]. 2010 Oct 7 [cited 2023 Sep 5];6(10):e1001134. Available from: https://dx.plos.org/10.1371/journal.ppat.1001134

27. Kacki S, Rahalison, Lila, Rajerison, Minoarisoa, Ferroglio, Ezio, Bianucci, Raffaella. Black Death in the rural cemetery of Saint-Laurent-de-la-Cabrerisse Aude-Languedoc, southern France, 14th century: immunological evidence. J Archaeol Sci. 2011;581–7.

28. Spyrou MA, Tukhbatova RI, Feldman M, Drath J, Kacki S, Beltrán de Heredia J, et al. Historical Y. pestis Genomes Reveal the European Black Death as the Source of Ancient and Modern Plague Pandemics. Cell Host Microbe [Internet]. 2016 Jun [cited 2023 Sep 19];19(6):874–81. Available from: http://linkinghub.elsevier.com/retrieve/pii/S1931312816302086

29. Brzobohatá H, Frolík J, Zazvonilová E. Bioarchaeology of Past Epidemic- and Famine-Related Mass Burials with Respect to Recent Findings from the Czech Republic. Interdiscip Archaeol - Nat Sci Archaeol [Internet]. 2019 Sep 10 [cited 2023 Sep 22];X(1):79–87. Available from: http://www.iansa.eu/papers/IANSA-2019-01-brzobohata.pdf

30. Haller M, Callan K, Susat J, Flux AL, Immel A, Franke A, et al. Mass burial genomics reveals outbreak of enteric paratyphoid fever in the Late Medieval trade city Lübeck. iScience [Internet]. 2021 May [cited 2023 Sep 4];24(5):102419. Available from: https://linkinghub.elsevier.com/retrieve/pii/S2589004221003874

31. Wiechmann, Ingrid, Harbeck, Michaela, Grupe, Gisela. Yersinia pestis DNA Sequences in Late Medieval Skeletal Finds, Bavaria. Emerg Infect Dis. 2010;16(11):1806–7.

32. Kahlow, S. Die Pest als Interpretationsproblem mittelalterlicher und frühneuzeitlicher Massengräber. Bull Société Suisse D'Anthropologie. 2007;13:97–104.

33. Wright R, Hanson, I., Sterenberg, J. The archaeology of mass graves. In: Forensic Archaeology: Advances in theory and practice. Routledge; 2005. p. 256.

34. Cannell RJS, Gustavsen L, Kristiansen M, Nau E. Delineating an Unmarked Graveyard by High-Resolution GPR and pXRF Prospection: The Medieval Church Site of Furulund in Norway. J Comput Appl Archaeol [Internet]. 2018 Mar 19 [cited 2023 Sep 24];1(1):1–18. Available from: http://journal.caa-international.org/articles/10.5334/jcaa.9/

35. Lütgert, S.A. Victims of the Great Famine and the Black Death? The archaeology of the mass graves found in the former graveyard of Holy Ghost Hospital, Lübeck (N. Germany), in the European context. Hikuin. 2000;27:255–64.

36. Dick HC, Pringle JK, Sloane B, Carver J, Wisniewski KD, Haffenden A, et al. Detection and characterisation of Black Death burials by multi-proxy geophysical methods. J Archaeol Sci [Internet]. 2015 Jul [cited 2023 Sep 4];59:132–41. Available from: https://linkinghub.elsevier.com/retrieve/pii/S0305440315001508

37. Conyers LB. Ground-Penetrating Radar Techniques to Discover and Map Historic Graves. Hist Archaeol [Internet]. 2006 Sep [cited 2023 Sep 19];40(3):64–73. Available from: http://link.springer.com/10.1007/BF03376733

38. Witten A, Brooks R, Fenner T. The Tulsa Race Riot of 1921: A geophysical study to locate a mass grave. Lead Edge [Internet]. 2001 Jun [cited 2023 Sep 18];20(6):655–60. Available from: http://library.seg.org/doi/10.1190/1.1439020

39. Hunter J, Cox M. Forensic archaeology: advances in theory and practice. London: Routledge; 2005.

40. Abate D, Sturdy Colls C, Moyssi N, Karsili D, Faka M, Anilir A, et al. Optimizing search strategies in mass grave location through the combination of digital technologies. Forensic Sci Int Synergy [Internet]. 2019 [cited 2023 Sep 18];1:95–107. Available from: https://linkinghub.elsevier.com/retrieve/pii/S2589871X19300828

41. Chetverikov B, Babiy L, Kuzyk Z, Zayats I. Comparison of 3D Models of Mass Graves Created on the Basis of Aerial Survey Data in 1944 and 2015. In: International Conference of Young Professionals «GeoTerrace-2022» [Internet]. Lviv, Ukraine,: European Association of Geoscientists & Engineers; 2022 [cited 2023 Sep 18]. p. 1–5. Available from: https://www.earthdoc.org/content/papers/10.3997/2214-4609.2022590080

42. Leblanc G, Kalacska M, Soffer R. Detection of single graves by airborne hyperspectral imaging. Forensic Sci Int [Internet]. 2014 Dec [cited 2023 Sep 18];245:17–23. Available from: https://linkinghub.elsevier.com/retrieve/pii/S0379073814003442

43. Moffat I. Locating Graves with Geophysics. In: Best practices of geoinformatic technologies for the mapping of archaeolandscapes. Archaeopress Publishing Ltd; 2015. p. 45–53. (Archaeopress archaeology).

44. Pringle JK, Jervis JR, Roberts D, Dick HC, Wisniewski KD, Cassidy NJ, et al. Long-term Geophysical Monitoring of Simulated Clandestine Graves using Electrical and Ground Penetrating Radar Methods: 4–6 Years After Burial. J Forensic Sci [Internet]. 2016 Mar [cited 2023 Sep 18];61(2):309–21. Available from: https://onlinelibrary.wiley.com/doi/10.1111/1556-4029.13009

45. Bolle, M. Die Wüstung Neuses am Roten Berg: Ein Beitrag zur Siedlungskunde mit 2 Tafeln und 2 Skizzen. Jahrb Akad Gemeinnütziger Wiss Zu Erf NF. 1937;53:57–85.

46. Holder-Egger, O. Monumenta Erphesfurtensia saec. XII. XIII. XIV. Hannover; 1899. 919 p. (Monumenta Germaniae Historica. Scriptores Rerum Germanicarum in usum scholarum).

47. Lehmann, Ernst. Der bronzezeitliche Friedhof auf dem Erfurter Flughafen. Mannus Z Für Vorgesch. 1928;Bd. 20 (special issue):1–78.

48. Seidel G, editor. Geologie von Thüringen: mit 34 Tabellen. 2., neubearbeitete Auflage. Stuttgart: E. Schweizerbart'sche Verlagsbuchhandlung (Nägele u. Obermiller); 2003. 601 p.

49. Bushart, M., Suck, R. Potenzielle Natürliche Vegetation Thüringens. Schriftenr Thür Landesanst Für Umw U Geol. 2008;78:1–139.

50. Beck HE, Zimmermann NE, McVicar TR, Vergopolan N, Berg A, Wood EF. Present and future Köppen-Geiger climate classification maps at 1-km resolution. Sci Data [Internet]. 2018 Oct 30 [cited 2024 Nov 26];5(1):180214. Available from: https://www.nature.com/articles/sdata2018214

51. Peel MC, Finlayson BL, McMahon TA. Updated world map of the Köppen-Geiger climate classification. Hydrol Earth Syst Sci [Internet]. 2007 Oct 11 [cited 2023 Sep 25];11(5):1633–44. Available from: https://hess.copernicus.org/articles/11/1633/2007/

52. Eifler, M. Cronica S. Petri Erfordensis moderna. In: The Encyclopedia of the Medieval Chronicle. Leiden - Bosten; 2010. p. 421–2.

53. Bauch, M., Wozniak, T. Erfurt. In: EpiMedDat [Internet]. 2024. Available from: http://epimeddat.net/index.php?title=Erfurt

54. Bolle, M. Die Kirche der Wüstung Neuseß. Ein Beitrag zur Wüstungskunde. Mitteilungen Ver Für Gesch Altertumskunde Von Erf. 1930;46:33–58.

55. Sczech K. Stadtarchäologischer Bericht über das Jahr 2012. Mitteilungen Ver Für Gesch Altertumskunde Von Erf NF 21. 2012;74:125–46.

56. Schmidt J, Voigt A, Seeburg V, Köhler A, Offermann M, Zielhofer C, et al. Georeferencing and other strategies to spatialise information from old maps – A collection of best practice recommendations [Internet]. Deutsches Archäologisches Institut, Römisch-Germanische Kommission; 2024 [cited 2024 Nov 27]. Available from: https://repo.dainst.org/de/dataset/georeferencing-and-other-strategies-to-spatialise-information-from-old-maps

57. Jones, G. Geophysical mapping of historic cemeteries. Tech Briefs Hist Archaeol. 2008;3:25–38.

58. Köhler A, Werban U, Pohle M, Rabiger-Völlmer J, Schneider B, Wanger-O'Neill A, et al. Determining carbon storage of a complex peat stratigraphy using non– and minimal-invasive geophysical prospection techniques (Verlorener Bach and Loosbach valleys, southern Germany). Geoderma [Internet]. 2024 Dec [cited 2024 Nov 27];452:117095. Available from: https://linkinghub.elsevier.com/retrieve/pii/S0016706124003240

59. Günther T, Rücker C, Spitzer K. Three-dimensional modelling and inversion of dc resistivity data incorporating topography - II. Inversion. Geophys J Int [Internet]. 2006 Aug [cited 2024 Aug 26];166(2):506–17. Available from: https://academic.oup.com/gji/article-lookup/doi/10.1111/j.1365-246X.2006.03011.x

60. Annan AP. Electromagnetic Principles of Ground Penetrating Radar. In: Ground Penetrating Radar Theory and Applications [Internet]. Elsevier; 2009 [cited 2024 Aug 26]. p. 1–40. Available from: https://linkinghub.elsevier.com/retrieve/pii/B9780444533487000016

61. Huisman JA, Hubbard SS, Redman JD, Annan AP. Measuring Soil Water Content with Ground Penetrating Radar: A Review. Vadose Zone J [Internet]. 2003 Nov [cited 2023 Dec 12];2(4):476–91. Available from: https://acsess.onlinelibrary.wiley.com/doi/10.2136/vzj2003.4760

62. Birkeland, P.W. Soils and geomorphology. Oxford: Oxford University Press; 1984. 372 p.

63. Ad-hoc-AG Boden. Bodenkundliche Kartieranleitung: mit 41 Abbildungen, 103 Tabellen und 31 Listen. 5., verbesserte und erweiterte Auflage. Stuttgart: In Kommission: E. Schweizerbart'sche Verlagsbuchhandlung (Nägele und Obermiller); 2005. 438 p.

64. Schad P. World Reference Base for Soil Resources—Its fourth edition and its history. J Plant Nutr Soil Sci [Internet]. 2023 Apr [cited 2023 Oct 1];186(2):151–63. Available from: https://onlinelibrary.wiley.com/doi/10.1002/jpln.202200417

65. Brown TA, Nelson DE, Vogel JS, Southon JR. Improved Collagen Extraction by Modified Longin Method. Radiocarbon [Internet]. 1988 [cited 2023 Oct 1];30(2):171–7. Available from: https://www.cambridge.org/core/product/identifier/S0033822200044118/type/journal_article

66. Wood R. From revolution to convention: the past, present and future of radiocarbon dating. J Archaeol Sci [Internet]. 2015 Apr [cited 2023 Oct 1];56:61–72. Available from: https://linkinghub.elsevier.com/retrieve/pii/S0305440315000576

67. Stuiver M, Polach HA. Discussion Reporting of ^{14} C Data. Radiocarbon [Internet]. 1977 [cited 2023 Oct 1];19(3):355–63. Available from: https://www.cambridge.org/core/product/identifier/S0033822200003672/type/journal_article

68. Reimer PJ. Composition and consequences of the IntCal20 radiocarbon calibration curve. Quat Res [Internet]. 2020 Jul [cited 2023 Oct 1];96:22–7. Available from: https://www.cambridge.org/core/product/identifier/S0033589420000423/type/journal_article

69. Bauer I, Endres W, Kerkhoff-Hader B, Koch R, Stephan HG, editors. Leitfaden zur Keramikbeschreibung: (Mittelalter - Neuzeit); Terminologie - Typologie - Technologie. 3. Aufl. München: Archäologische Staatssammlung; 2005. 198 p. (Kataloge der Archäologischen Staatssammlung München Beiheft).

70. Lüdtke H, Schietzel K. Handbuch zur mittelalterlichen Keramik in Nordeuropa. Neumünster: Wachholtz; 2001. (Schriften des archäologischen Landesmuseums).

71. Timpel W. Mittelalterliche Keramik im westlichen Thüringen, 8.-12. Jahrhundert. Weimar: Museum für Ur- und Frühgeschichte Thüringens; 1990. 114 p. (Weimarer Monographien zur Ur- und Frühgeschichte).

72. Vandenberghe J. The fluvial cycle at cold–warm–cold transitions in lowland regions: A refinement of theory. Geomorphology [Internet]. 2008 Jun [cited 2024 Sep 9];98(3–4):275–84. Available from: https://linkinghub.elsevier.com/retrieve/pii/S0169555X07002358

73. Busschers FS, Kasse C, Van Balen RT, Vandenberghe J, Cohen KM, Weerts HJT, et al. Late Pleistocene evolution of the Rhine-Meuse system in the southern North Sea basin: imprints of climate change, sea-level oscillation and glacio-isostacy. Quat Sci Rev [Internet]. 2007 Dec [cited 2024 Sep 13];26(25–28):3216–48. Available from: https://linkinghub.elsevier.com/retrieve/pii/S0277379107002004

74. Kasse C, Vandenberghe J, Van Huissteden J, Bohncke SJP, Bos JAA. Sensitivity of Weichselian fluvial systems to climate change (Nochten mine, eastern Germany). Quat Sci Rev [Internet]. 2003 Oct [cited 2024 Sep 13];22(20):2141–56. Available from: https://linkinghub.elsevier.com/retrieve/pii/S027737910300146X

75. Mol J, Vandenberghe J, Kasse C. River response to variations of periglacial climate in mid-latitude Europe. Geomorphology [Internet]. 2000 Jun [cited 2024 Sep 9];33(3–4):131–48. Available from: https://linkinghub.elsevier.com/retrieve/pii/S0169555X99001269

76. Starkel L, Ge¸bica P, Superson J. Last Glacial–Interglacial cycle in the evolution of river valleys in southern and central Poland. Quat Sci Rev [Internet]. 2007 Nov [cited 2024 Oct 18];26(22–24):2924–36. Available from: https://linkinghub.elsevier.com/retrieve/pii/S0277379107002557

77. Winsemann J, Lang J, Roskosch J, Polom U, Böhner U, Brandes C, et al. Terrace styles and timing of terrace formation in the Weser and Leine valleys, northern Germany: Response of a fluvial system to climate change and glaciation. Quat Sci Rev [Internet]. 2015 Sep [cited 2024 Sep

9];123:31–57. Available from: https://linkinghub.elsevier.com/retrieve/pii/S0277379115300159

78. Fischer P, Hambach U, Klasen N, Schulte P, Zeeden C, Steininger F, et al. Landscape instability at the end of MIS 3 in western Central Europe: evidence from a multi proxy study on a Loess-Palaeosol-Sequence from the eastern Lower Rhine Embayment, Germany. Quat Int [Internet]. 2019 Jan [cited 2024 Sep 9];502:119–36. Available from: https://linkinghub.elsevier.com/retrieve/pii/S1040618217305979

79. Krauß L, Zens J, Zeeden C, Schulte P, Eckmeier E, Lehmkuhl F. A Multi-Proxy Analysis of two Loess-Paleosol Sequences in the Northern Harz Foreland, Germany. Palaeogeogr Palaeoclimatol Palaeoecol [Internet]. 2016 Nov [cited 2024 Sep 13];461:401–17. Available from: https://linkinghub.elsevier.com/retrieve/pii/S0031018216304230

80. Van Huissteden K o, Pollard D. Oxygen isotope stage 3 fluvial and eolian successions in Europe compared with climate model results. Quat Res [Internet]. 2003 Mar [cited 2024 Sep 9];59(2):223–33. Available from: https://www.cambridge.org/core/product/identifier/S0033589400011868/type/journal_article

81. Eberle J, Eitel B, Blümel WD, Wittmann P. Deutschlands Süden - vom Erdmittelalter zur Gegenwart [Internet]. Berlin, Heidelberg: Springer Berlin Heidelberg; 2017 [cited 2024 Sep 13]. 195 p. Available from: http://link.springer.com/10.1007/978-3-662-54381-8

82. Kirchner A, Karaschewski J, Schulte P, Wunderlich T, Lauer T. Latest Pleistocene and Holocene Floodplain Evolution in Central Europe—Insights from the Upper Unstrut Catchment (NW-Thuringia/Germany). Geosciences [Internet]. 2022 Aug 19 [cited 2023 Sep 4];12(8):310. Available from: https://www.mdpi.com/2076-3263/12/8/310

83. Terhorst B. Periglacial cover beds and soils in landslide areas of SW-Germany. CATENA [Internet]. 2007 Dec [cited 2024 Sep 13];71(3):467–76. Available from: https://linkinghub.elsevier.com/retrieve/pii/S034181620700046X

84. Antoine P, Rousseau DD, Moine O, Kunesch S, Hatté C, Lang A, et al. Rapid and cyclic aeolian deposition during the Last Glacial in European loess: a high-resolution record from Nussloch, Germany. Quat Sci Rev [Internet]. 2009 Dec [cited 2024 Sep 13];28(25–26):2955–73. Available from: https://linkinghub.elsevier.com/retrieve/pii/S0277379109002674

85. Meszner S, Kreutzer S, Fuchs M, Faust D. Late Pleistocene landscape dynamics in Saxony, Germany: Paleoenvironmental reconstruction using loess-paleosol sequences. Quat Int [Internet]. 2013 May [cited 2024 Sep 13];296:94–107. Available from: https://linkinghub.elsevier.com/retrieve/pii/S1040618213000050

86. Kleber A, Terhorst B, Bullmann H, Damm B, Dietze M, Döhler S, et al. Subdued mountains of Central Europe. In: Mid-Latitude Slope Deposits (Cover Beds) [Internet]. Elsevier; 2024 [cited 2024 Sep 29]. p. 9–114. Available from: https://linkinghub.elsevier.com/retrieve/pii/B9780323960038000116

87. Lauer T, Von Suchodoletz H, Vollmann H, Meszner S, Frechen M, Tinapp C, et al. Landscape aridification in Central Germany during the late Weichselian Pleniglacial - results from the Zauschwitz loess site in western Saxony. Z Für Geomorphol Suppl Issues [Internet]. 2014 Feb 1 [cited 2024 Sep 13];58(1):27–50. Available from: http://www.schweizerbart.de/papers/zfg_suppl/detail/58/81991/Landscape_aridification_in_Central_Germany_during_?af=crossref

88. Lehmkuhl F, Zens J, Krauß L, Schulte P, Kels H. Loess-paleosol sequences at the northern European loess belt in Germany: Distribution, geomorphology and stratigraphy. Quat Sci Rev [Internet]. 2016 Dec [cited 2024 Sep 27];153:11–30. Available from: https://linkinghub.elsevier.com/retrieve/pii/S0277379116304383

89. Sprafke T, Schulte P, Meyer-Heintze S, Händel M, Einwögerer T, Simon U, et al. Paleoenvironments from robust loess stratigraphy using high-resolution color and grain-size data of the last glacial Krems-Wachtberg record (NE Austria). Quat Sci Rev [Internet]. 2020 Nov [cited 2024 Sep 27];248:106602. Available from: https://linkinghub.elsevier.com/retrieve/pii/S0277379120305643

90. Geßlein B, Schellmann G. Jungquartäre Flussterrassen am mittleren Lech zwischen Kinsau und Klosterlechfeld – Erste Ergebnisse. EG Quat Sci J [Internet]. 2011 Nov 17 [cited 2024 Sep 29];60(4):400–13. Available from: https://egqsj.copernicus.org/articles/60/26/2011/

91. Schirmer, Wolfgang. Edifice of Fluvial Terrace Flights, Stacks and Rows. Geosciences [Internet]. 2020 Dec 15 [cited 2023 Sep 4];10(12):501. Available from: https://www.mdpi.com/2076-3263/10/12/501

92. Altermann M, Rinklebe J, Merbach I, Körschens M, Langer U, Hofmann B. Chernozem—Soil of the Year 2005. J Plant Nutr Soil Sci [Internet]. 2005 Dec [cited 2023 Sep 4];168(6):725–40. Available from: https://onlinelibrary.wiley.com/doi/10.1002/jpln.200521814

93. Dreibrodt S, Hofmann R, Dal Corso M, Bork HR, Duttmann R, Martini S, et al. Earthworms, Darwin and prehistoric agriculture-Chernozem genesis reconsidered. Geoderma [Internet]. 2022 Mar [cited 2023 Sep 4];409:115607. Available from: https://linkinghub.elsevier.com/retrieve/pii/S001670612100687X

94. Eckmeier E, Gerlach R, Gehrt E, Schmidt MWI. Pedogenesis of Chernozems in Central Europe — A review. Geoderma [Internet]. 2007 May [cited 2023 Sep 4];139(3–4):288–99. Available from: https://linkinghub.elsevier.com/retrieve/pii/S0016706107000201

95. Lorz C, Saile T. Anthropogenic pedogenesis of Chernozems in Germany? – A critical review. Quat Int [Internet]. 2011 Oct [cited 2023 Sep 4];243(2):273–9. Available from: https://linkinghub.elsevier.com/retrieve/pii/S1040618210004519

96. Vysloužilová B, Ertlen D, Schwartz D, Šefrna L. Chernozem. From concept to classification: a review. AUC Geogr [Internet]. 2016 Jun 22 [cited 2023 Sep 4];51(1):85–95. Available from: http://www.karolinum.cz/doi/10.14712/23361980.2016.8

97. Von Suchodoletz H, Van Meer M, Kühn P, Wiedner K, Schunke T, Reimann T. Deciphering timing and rates of Central German Chernozem/Phaeozem formation through high resolution single-grain luminescence dating. Sci Rep [Internet]. 2023 Mar 23 [cited 2024 Sep 29];13(1):4769. Available from: https://www.nature.com/articles/s41598-023-32005-9

98. Von Suchodoletz H, Tinapp C, Lauer T, Glaser B, Stäuble H, Kühn P, et al. Distribution of Chernozems and Phaeozems in Central Germany during the Neolithic period. Quat Int [Internet]. 2019 Mar [cited 2024 Sep 29];511:166–84. Available from: https://linkinghub.elsevier.com/retrieve/pii/S1040618217303129

99. Kleber M, Röner J, Chenu C, Glaser B, Knicker H, Jahn R. PREHISTORIC ALTERATION OF SOIL PROPERTIES IN A CENTRAL GERMAN CHERNOZEMIC SOIL: IN SEARCH OF PEDOLOGIC

INDICATORS FOR PREHISTORIC ACTIVITY. Soil Sci [Internet]. 2003 Apr [cited 2024 Sep 29];168(4):292–306. Available from: http://journals.lww.com/00010694-200304000-00006

100. Schirmer, Wolfgang. Valley bottoms in the late Quaternary. Z Für Geomorphol Suppl. 1995;100:27–51.

101. Schirmer, Wolfgang. Die Talentwicklung an Main und Regnitz seit dem Hochwurm. Geol Jb. 1983;A 71:11–43.

102. Rittweger H. The "Black Floodplain Soil" in the Amöneburger Becken, Germany: a lower Holocene marker horizon and indicator of an upper Atlantic to Subboreal dry period in Central Europe? CATENA [Internet]. 2000 Sep [cited 2023 Sep 4];41(1–3):143–64. Available from: https://linkinghub.elsevier.com/retrieve/pii/S0341816200001132

103. Houben P. Geomorphological facies reconstruction of Late Quaternary alluvia by the application of fluvial architecture concepts. Geomorphology [Internet]. 2007 Apr [cited 2024 Sep 29];86(1–2):94–114. Available from: https://linkinghub.elsevier.com/retrieve/pii/S0169555X06003849

104. Notebaert B, Houbrechts G, Verstraeten G, Broothaerts N, Haeckx J, Reynders M, et al. Fluvial architecture of Belgian river systems in contrasting environments: implications for reconstructing the sedimentation history. Neth J Geosci - Geol En Mijnb [Internet]. 2011 Aug [cited 2024 Sep 29];90(1):31–50. Available from: https://www.cambridge.org/core/product/identifier/S0016774600000652/type/journal_article

105. Tinapp C, Heinrich S, Herbig C, Schneider B, Stäuble H, Miera J, et al. Holocene floodplain evolution in a central European loess landscape – geoarchaeological investigations of the lower Pleiße valley in NW Saxony. EG Quat Sci J [Internet]. 2019 Jul 15 [cited 2024 Jul 29];68(2):95–105. Available from: https://egqsj.copernicus.org/articles/68/95/2019/

106. Von Suchodoletz H, Khosravichenar A, Fütterer P, Zielhofer C, Schneider B, Sprafke T, et al. Holocene overbank sedimentation in Central Europe between natural and human drivers - The Weiße Elster River (Central Germany). Geomorphology [Internet]. 2024 Mar [cited 2024 Sep 29];449:109067. Available from: https://linkinghub.elsevier.com/retrieve/pii/S0169555X24000175

107. Kay JE, Koncz I. Archaeological Approaches to Multiple Burials and Mass Graves in Early Medieval Europe. Mediev Archaeol [Internet]. 2023 Jan 2 [cited 2024 Feb 27];67(1):115–36. Available from: https://www.tandfonline.com/doi/full/10.1080/00766097.2023.2204667

108. Krauße, Lars. Ausgrabung "Zum Zoopark" in Erfurt von Mai bis August 2012. Weimar: Thuringian State Office for Monument Preservation and Archaeology; 2012 p. 1–5. Report No.: VG-Nr.: 12/107.

109. Kirchhoff A. Die Lagenverhältnisse von Erfurt. Mitth Ver Für Erdkd Zu HalleS [Internet]. 1895 [cited 2024 Oct 3];19:1–12. Available from: https://opendata.uni-halle.de//handle/1981185920/91444

110. Schoenen D, Albrecht MC. Die Verwesung aus hygienischer und bodenkundlicher Sicht. Berlin; 2003. 134 p. (Schriftenreihe des Vereins für Wasser-, Boden- und Lufthygiene e.V.; vol. 113).

111. Williams A, Temple T, Pollard SJ, Jones RJA, Ritz K. Environmental Considerations for Common Burial Site Selection After Pandemic Events. In: Ritz K, Dawson L, Miller D, editors. Criminal and

Environmental Soil Forensics [Internet]. Dordrecht: Springer Netherlands; 2009 [cited 2024 Oct 2]. p. 87–101. Available from: http://link.springer.com/10.1007/978-1-4020-9204-6_7

112. O'Sullivan D. Burial of the Christian Dead in the Later Middle Ages. In: The Oxford Handbook of the Archaeology of Death and Burial [Internet]. Oxford University Press; 2013 [cited 2024 Oct 1]. p. 259–80. Available from: https://academic.oup.com/edited-volume/38604/chapter/334707878

113. Vivas M. Christian Burial Privation in the Middle Ages: an interdisciplinary approach (France, mid-10th–early 14th) [Internet]. Edicions de la Universitat de Lleida; 2018 [cited 2024 Oct 1] p. 191–210. Available from: http://hdl.handle.net/10459.1/65937

114. Larson DO, Vass AA, Wise M. Advanced Scientific Methods and Procedures in the Forensic Investigation of Clandestine Graves. J Contemp Crim Justice [Internet]. 2011 May [cited 2024 Nov 4];27(2):149–82. Available from: https://journals.sagepub.com/doi/10.1177/1043986211405885

115. Ruffell A, McCabe A, Donnelly C, Sloan B. Location and Assessment of an Historic (150–160 Years Old) Mass Grave Using Geographic and Ground Penetrating Radar Investigation, NW Ireland*. J Forensic Sci [Internet]. 2009 Mar [cited 2024 Nov 4];54(2):382–94. Available from: https://onlinelibrary.wiley.com/doi/10.1111/j.1556-4029.2008.00978.x

116. Dick HC, Pringle JK, Wisniewski KD, Goodwin J, Van Der Putten R, Evans GT, et al. Determining geophysical responses from burials in graveyards and cemeteries. GEOPHYSICS [Internet]. 2017 Nov 1 [cited 2024 Nov 5];82(6):B245–55. Available from: https://library.seg.org/doi/10.1190/geo2016-0440.1

117. Berezowski V, Mallett X, Ellis J, Moffat I. Using Ground Penetrating Radar and Resistivity Methods to Locate Unmarked Graves: A Review. Remote Sens [Internet]. 2021 Jul 23 [cited 2024 Nov 4];13(15):2880. Available from: https://www.mdpi.com/2072-4292/13/15/2880

118. Bevan BW. The search for graves. GEOPHYSICS [Internet]. 1991 Sep [cited 2024 Nov 4];56(9):1310–9. Available from: https://library.seg.org/doi/10.1190/1.1443152

119. Sherrod L, Willever H, Shollenberger K, Potter C, Thorne R, Kline A. Geophysical Investigations of United States Revolutionary War Era (1777–1778) Mass Burial Sites in Pennsylvania, USA. J Environ Eng Geophys [Internet]. 2020 Dec [cited 2024 Nov 4];25(4):477–96. Available from: https://library.seg.org/doi/10.32389/JEEG20-023

120. Kirchner A, Zielhofer C, Werther L, Schneider M, Linzen S, Wilken D, et al. A multidisciplinary approach in wetland geoarchaeology: Survey of the missing southern canal connection of the Fossa Carolina (SW Germany). Quat Int [Internet]. 2018 Apr [cited 2024 Dec 4];473:3–20. Available from: https://linkinghub.elsevier.com/retrieve/pii/S1040618217308996

121. Von Suchodoletz H, Pohle M, Khosravichenar A, Ulrich M, Hein M, Tinapp C, et al. The fluvial architecture of buried floodplain sediments of the Weiße Elster River (Germany) revealed by a novel method combination of drill cores with two-dimensional and spatially resolved geophysical measurements. Earth Surf Process Landf [Internet]. 2022 Mar 30 [cited 2024 Nov 7];47(4):955–76. Available from: https://onlinelibrary.wiley.com/doi/10.1002/esp.5296

122. Brown AG. The use of forensic botany and geology in war crimes investigations in NE Bosnia. Forensic Sci Int [Internet]. 2006 Nov [cited 2024 Nov 4];163(3):204–10. Available from: https://linkinghub.elsevier.com/retrieve/pii/S037907380600288X

123. Reeder P, Jol H, McClymont A, Bauman P, Barrow M. Using Geophysics to Locate Holocaust Era Mass Graves in Jewish Cemeteries: Examples from Latvia and Lithuania. Heritage [Internet]. 2024 Jul 16 [cited 2024 Nov 4];7(7):3766–98. Available from: https://www.mdpi.com/2571-9408/7/7/179

124. Rubio-Melendi D, Gonzalez-Quirós A, Roberts D, García García MDC, Caunedo Domínguez A, Pringle JK, et al. GPR and ERT detection and characterization of a mass burial, Spanish Civil War, Northern Spain. Forensic Sci Int [Internet]. 2018 Jun [cited 2024 Nov 4];287:e1–9. Available from: https://linkinghub.elsevier.com/retrieve/pii/S0379073818301312

Supplementary Information

What the landscape can tell: An integrative stratigraphic prospection approach for localizing a Black Death mass grave in Erfurt/Central Germany

Michael Hein, Nik Usmar, Annabell Engel, Johannes Rabiger-Völlmer, Johannes Schmidt, Matthias Silbermann, Marco Pohle, Lukas Werther, Birgit Schneider, Christian Tannhäuser, Alexander Herbig, Jan Nováček, Ulrike Werban, Martin Bauch, Christoph Zielhofer

Contents:

Supplementary Section 1 – Former wetlands in the study area implied by old maps

On the old topographic map of 1839 (SI Fig. 1A), south of the "Roter Berg" and overlapping with the southwestern part of our study area (red square), extensive wetlands are documented, also indicated by the toponyms Rieth-Feld (reed field) and Nonnen-Erlen (nuns' alders). Later accounts report on stagnant water bodies as the result of peat cutting before the area was drained in the later 19th century (Lehmann, 1928; Kirchoff, 1885). On the geological map of 1931 (SI Fig. 1B), roughly the same former wetland area is designated as overbank deposits of the river Gera, which deviates from the smaller extent of these overbank fines in today's data (compare Fig.1, main text).

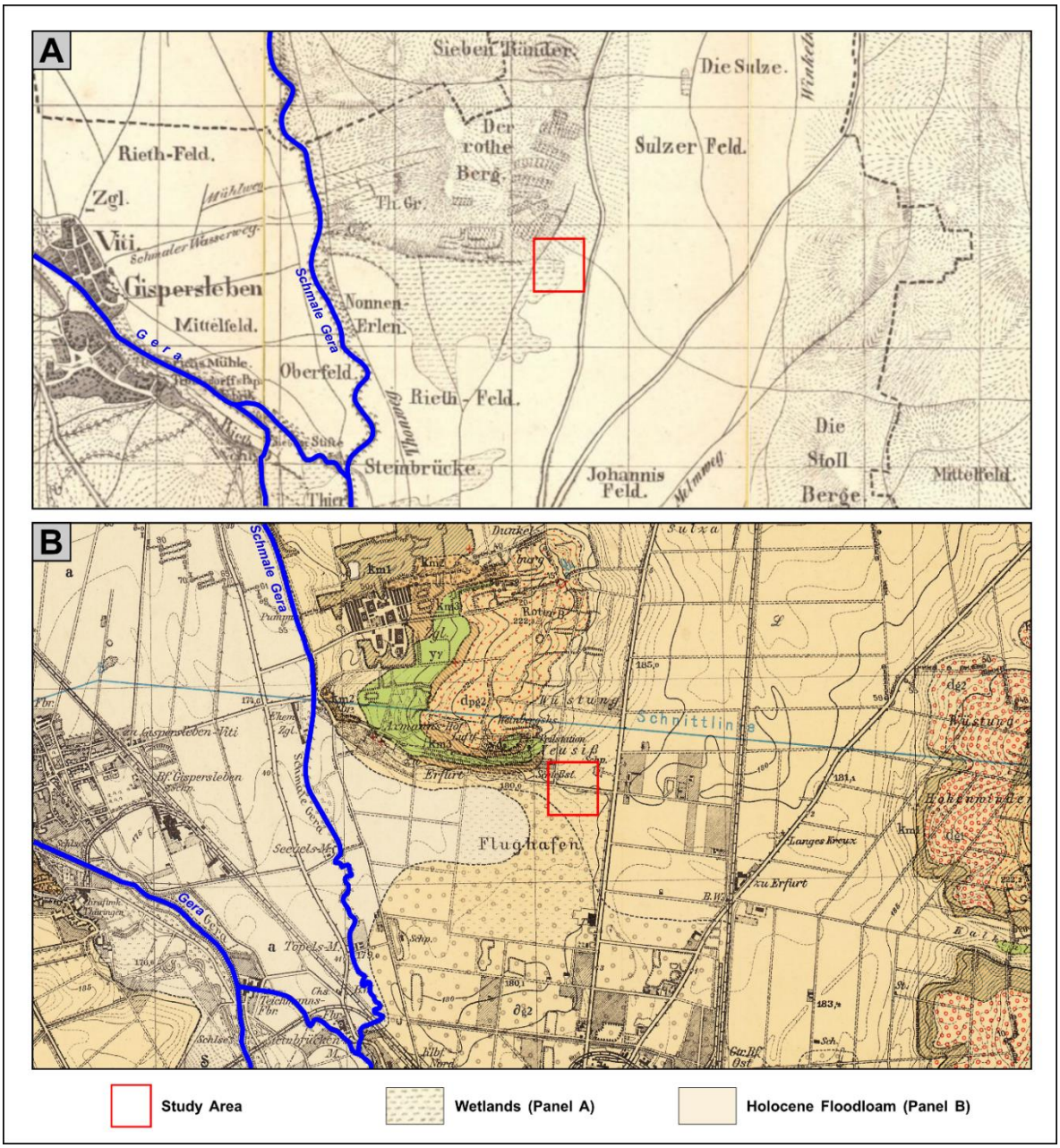

SI Fig. 1: A – Topographic map 1:25000 from 1839, created and designed by von Zittwitz and Uckermann (permalink: http://www.deutschefotothek.de/documents/obj/70301944). It documents wetland areas in the SW part of the study area. **B** – Geological map 1:25000 from 1931, edited by A. Reichardt and published by the Prussian Geological Survey, Berlin. It indicates more extensive areas of overbank deposits/floodloam than today (compare Fig. 1, main text).

Supplementary Section 2 – Locating the features of the excavation in 1926/27

The georeferencing of the excavation sketch by Bolle (1937) (SI Fig. 2; Fig. 2, main text) provides important information on the location of the church and its surroundings in Neuses. The sketch shows mass graves (Mgr.), individual graves (Egr.), the cemetery wall (FM) and the rubble (B(schematisch)) of the former church. Due to the lack of a coordinate system, however, localization was a particular challenge. The referencing (a, b, c) was carried out using control points on prominent landmarks. This resulted in two variants. The western variant (a + b) locates the sketch via the road junction in the northwest and via the ends of the presumed cemetery wall, which was supposedly visible as an elevation in the DEM. The length of the DEM elevation corresponds approximately to the information (25 m) on the sketch. The eastern variant (a + c) is based on the distances to the surrounding streets in the north (40 m) and east (190 m) of the sketch, which still bear the same names today. The distances were converted into control points for georeferencing using auxiliary lines. The eastern variant was given greater consideration in the planning of the transects for soil mapping due to its specific dimensions, which later proved to be correct.

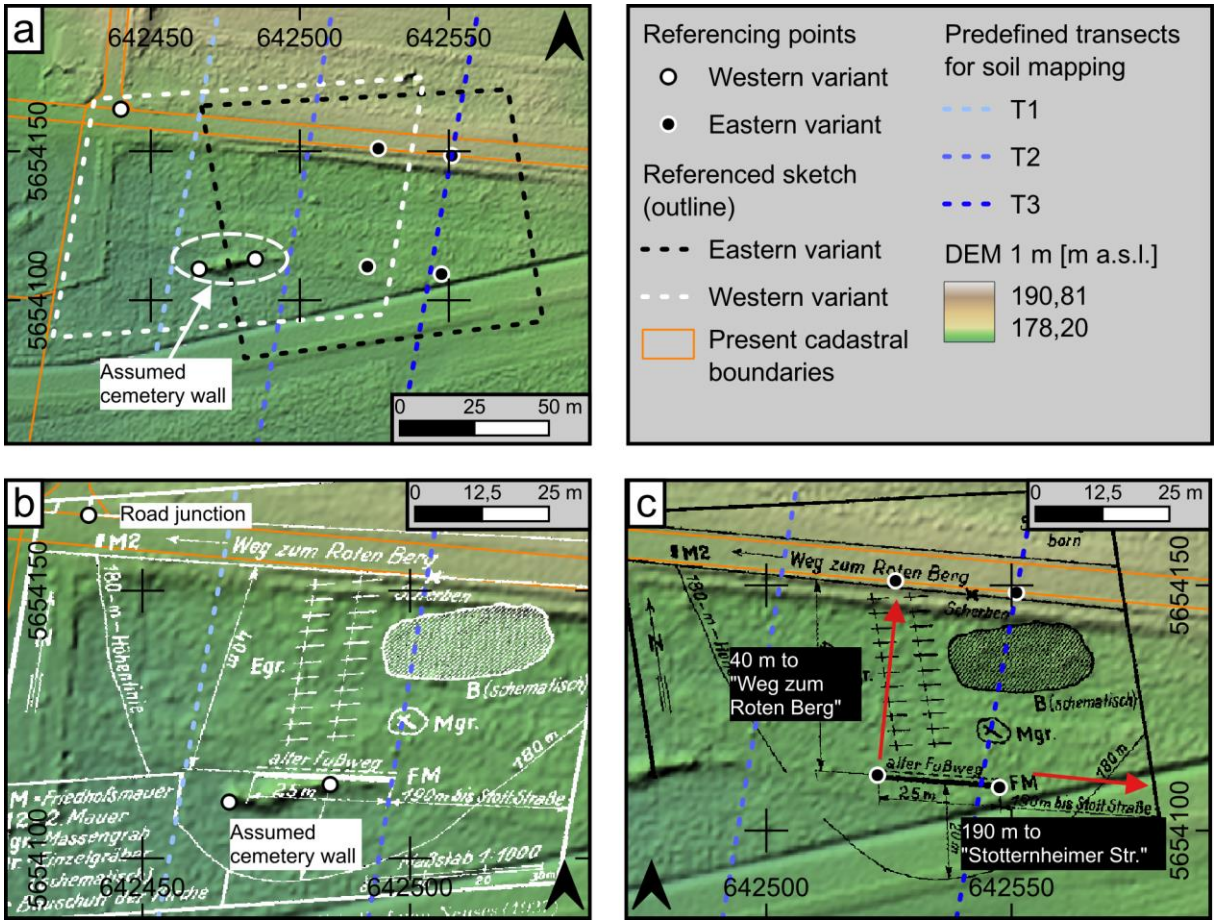

SI Fig. 2: a - Two variants for georeferencing the excavation sketch by Bolle (1937). **b** – Western variant hinged on the road junction in the north and the (incorrectly assumed) representation of the former cemetery wall in the DEM. **c** – The preferred eastern variant, mainly based on the distances to the surrounding roads as indicated by Bolle (1937). Digital elevation model DEM1 coutesy of Thuringian State Office for Land Management and Geoinformation

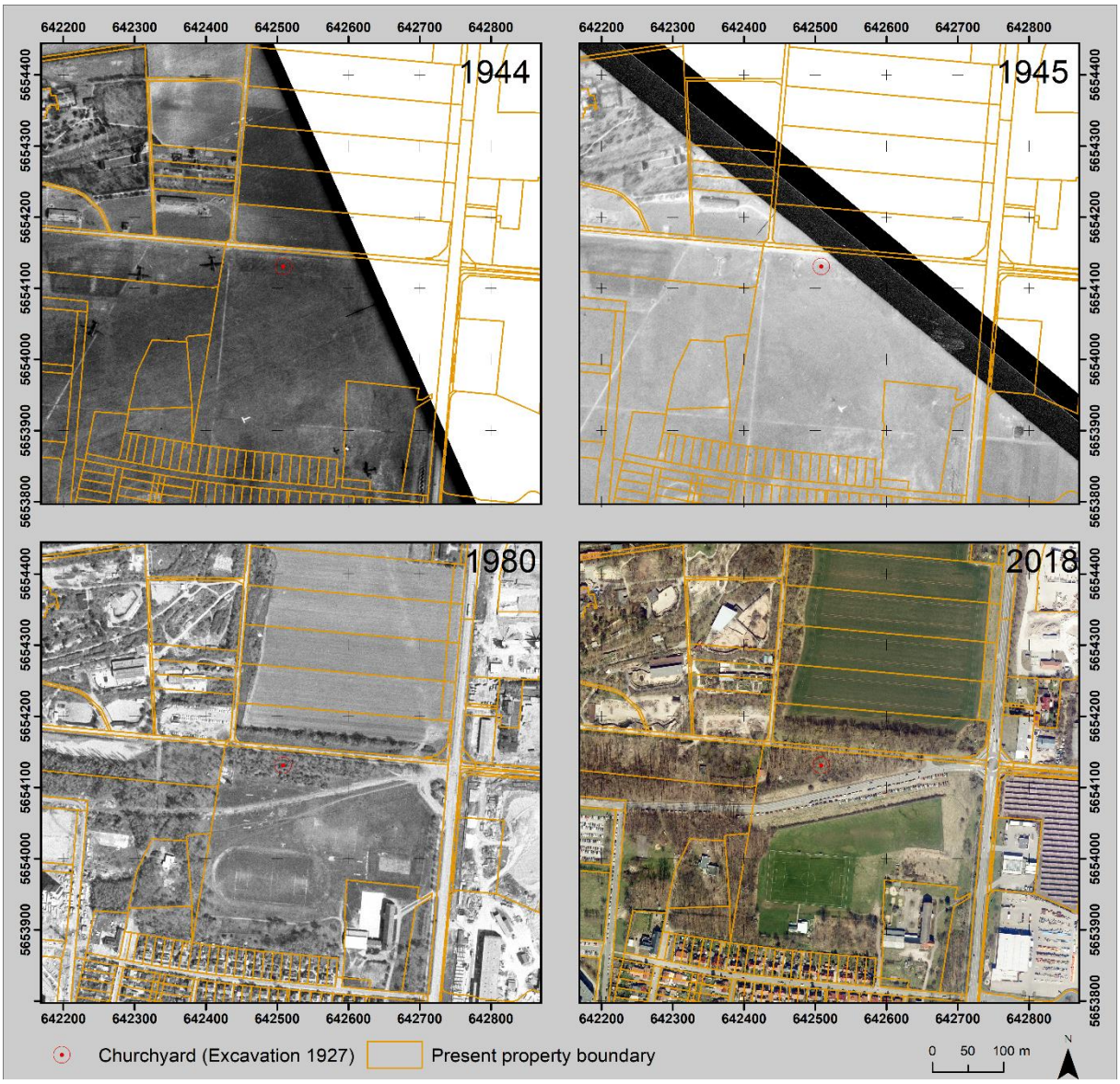

SI Fig. 3: Aerial photographs of the study area and its sourroundings from the years 1944, 1945, 1980 and 2018 (courtesy of Thuringian State Office for Land Management and Geoinformation, with property boundaries taken from the Cadastre Information System ALKIS, 2019). Note the increase of infrastructure and building structures over time. The study area (around the red dot) was largely spared from construction with only a distinct vegetation change noticable.

The aerial photographs from 1944, 1945, 1980 and 2018 (SI Fig. 3) show that the territory around the churchyard (red dot) of the deserted village Neuses. From 1927 to 1945, the area was situated at the northern margin of the first airfield of the City of Erfurt. Today, the area has been incorporated into Erfurt as the city has grown, whereas the presumed position of the churchyard itself (red dot) has not been a site of construction and fortunately is accessible for geophysical and geoarchaeological investigations.

Supplementary Section 3 – Detailed stratigraphic information

3.1 Chernozem zone

Stratigraphic Unit 1 (SU1): In this area, the lowermost deposit we discovered is a mudstone sequence from the Weser formation in the Middle Keuper period, exposed in the cores EN-RK 1, 36, 41, 55 and 58 (Figs. 3 and 5, main text). This clayey-silty unconsolidated deposit is vastly non-calcareous, massive to finely-laminated and free of pebbles. Its color varies greatly from mostly reddish brown to dark red, pale olive and greenish grey (Munsell colors from 10R 5/2 and 2,5YR 4/3 to 6/5 BG), which is in accordance with the known polychrome character of this formation in the wider region (1). The upper boundary of SU1 is usually situated at 175-177 m asl in our boreholes. In the ERT profiles, this unit is characterized by low resistivity values up to 60 Ωm (Fig. 6 and 8, main text; ERT profiles 2, 3, 6 and 7 as well as P11/12, SI Fig. 4).

Stratigraphic Unit 2 (SU2): Unconformably overlying the Keuper mudstone is a gravelly and calcareous sand encountered in the cores EN-RK 3, 4, 7, 19, 36-38, 40, 42, 47, 51, 53 and 55-58. Only in two positions, the deposit has been drilled through completely with respective thicknesses of ~2 m (EN-RK 36 and 58, see. Fig. 4, main text). It consists of a reddish brown (Munsell colors mostly between 5YR 5/2 and 5/5), poorly-sorted fine to coarse sand with varying gravel contents between 10 and 50%, the latter fraction featuring well-rounded pebbles of mainly quartz, chert, rhyolite and limestone. Occasionally, loamy sections exist in this layer that likely represent redeposited material derived from the Keuper mudstone SU1. As a tendency, the upper boundary of SU2 is slightly inclined to the south from just over 178 m to just under 177 m asl in the investigated area. SU2 is cautiously interpreted as the Weichselian fluvial gravel of the “lower terrace”, or German: “Niederterrasse”. In the ERT profiles, the coarse material of this unit and its poor sorting are reflected by high resistivity values up to 400 Ωm (Fig. 6, main text; ERT profiles 2 and 3 and SI Fig. 4).

Stratigraphic Unit 3 (SU3): In all the boreholes of this zone, the stratigraphic superposition of the SU2 gravels is formed by a heterogeneous loamy to clayey slope deposit. Its fine-grained texture and the variegated colors – reddish brown to olive yellow (mostly 2,5YR 3/4 to 5YR 6/2) – are strongly reminiscent of the Keuper mudstone SU1. The same applies to the seemingly random changes in the structural composition between massive and finely-laminated sections. The main differences to SU1 apart from the significantly detached stratigraphic position are (i) a certain (fine) sand content, (ii) a noticeable carbonate content of an estimated 2-5 %, (iii) the admixture of up to 15 % well-rounded pebbles – mainly quartz and rhyolite, and (iv) the occasional occurrence of loessic interlayers in a mm- to dm-range (e.g. EN-RK 5, Fig. 5, main text). SU3 has been fully exposed in cores EN-RK 3, 4, 7, 19, 37, 40, 42, 50, 51, 53, and 57-58. Its thickness fluctuates between 90 cm and >3.5 m (cores EN-RK 51 and 5) with a clear tendency to decrease downslope to the south and the east, while its upper boundary is usually

subparallel to the surface at 1 to 2 m depth. All of the above properties justify the categorization as a periglacial slope debris/deposit.

Stratigraphic Unit 4 (SU4): This widespread unit is characterized by an alternate bedding and partial mixture of the underlying SU3 and the overlying loess deposit. These two parent materials appear in variable proportions both within and between the core sequences: From sporadic reddish and loamy streaks inside an otherwise loess-like sediment to rhythmically-bedded 2 cm alternations of both members to more homogenized and reddish mixtures of both components but with isolated bands of reworked loess-like material. Therefore, in terms of texture and color, co-occurrences and mixtures ranging from light brown sandy silt to reddish brown loamy clay can be found (Munsell colors 7,5 YR 6/5 to 2,5YR 4/4). Usually however, the lower parts of SU4 are more closely related to the underlying deposit and *vice versa*. Since both end-members involved are calcareous, the same is true for SU4, with estimated carbonate contents between 5 and 10 %. The thicknesses vary between 20 and 90 cm, with the lower boundaries following the surface in a subparallel manner and being situated at 1.4 to 1.8 m depth on average. In many cases, these lower boundaries are marked by an accumulation of pebbly components, indicating a possible truncation of the underlying SU3 prior to the deposition of SU4 (e.g. cores EN-RK 5, 7, 23, 29, 58). Conversely, the upper boundary is not as distinct, but rather represented by a gradual transition to the overlying loess of SU5. The stratigraphic unit SU4 is missing in the cores EN-RK 3, 4 and 6 for what we assume to be natural causes and additionally in most cores located in the area particularly affected by soil removal during the construction of the airfield in 1926/27, including EN-RK 22, 37-40, 42-45 and 51-54 (Fig 5.). We interpret SU4 to be the product of periglacial slopewash processes and refer to it as reworked loess or colluvial loess.

Stratigraphic Unit 5 (SU5): This unit encompasses the near-surface unstratified loess-like deposits and the chernozemic soils that formed within this substrate, and it is thus subdivided into SU5.1 and SU5.2. Originally and according to strictly natural distribution, this unit occurs in all boreholes within this zone.

SU5.1: Conformably above the reworked loess of SU4, a 15 to 72 cm thick layer of coherent and seemingly unstructured loess-like deposits occurs. The sediment is light (reddish) brown in color (10YR 6/5 to 7,5YR 5/4), mainly silty and slightly fine-sandy/loamy, always highly calcareous with estimated carbonate contents of ≥10 % and also contains secondary carbonates, namely pseudomycelia and occasional loess dolls. Plausibly, it represents primary aeolian loess, but as processes of post-depositional modifications, such as cryogenesis and slight reworking, cannot be completely ruled out based on our findings, we will henceforth refer to it more generally as “loess”. Positions where this loess layer is missing in the chernozem zone are the central segments of transects 3 (EN-RK 52-54) and especially transect 2 (e.g. EN-RK 42-45), because it was removed there for the construction and levelling of the

airfield in 1926/27, and additionally locations with deep archaeological features that incorporate the loess (e.g. EN-RK 19, 25 and 27) (Fig. 5, main text).

SU5.2: Within the loess, a chernozem has formed with thicknesses of the chernic horizon between 45 and 90 cm. This is typically followed by a ca. 10-20 cm transitional A-C horizon below. Both of these horizons, as well as the underlying loess show distinct traces of bioturbation in the form of filled earthworm channels (nearly in all cores) and tunnels of burrowing mammals, i.e. krotovinas, e.g. in EN-RK 8, 9, 22 and 26. The chernic horizon has a granular structure, is dark brown to very dark greyish brown in color (10YR 3/3 to 7,5YR 3/2) and in some cases nearly decalcified (e.g. EN-RK 8, 10, 18, 24, 28, 29), but mostly, the carbonate contents are estimated to 2-10% (e.g. EN-RK 3-7, 23, 26, 58). At a few positions, the apparent formation of an incipient clay-humus enriched B-horizon can be observed, therefore justifying the designation of the solum as luvic phaeozem there (e.g. EN-RK 29). Whether the small-scale co-existence of (haplic/calcic) chernozems and (luvic) phaeozems is an expression of natural pedogenic variability or rather of structural anthropogenic interventions is not within the scope of this research and will be addressed during future investigations, when also soil profiles will be available. In the context of this study, however, the humic topsoil of this zone will be more generally referred to as “chernozem” or “chernic horizon”. Just as for the loess, the chernozem is missing in the central part of the AOI (transects T2 and T3) due to modern soil removal, and in those position where it was consumed by deep archaeological features (e.g. EN-RK 19-21, 25 and 27).

Within the ERT profiles, the rather fine-grained stratigraphic units SU3-SU5 appear as an almost constant and amalgamated layer with resistivity values of 50 to 150 Ωm. In contrast to the borehole stratigraphy, a clear subdivision is not possible in the ERT (Fig. 6, main text; ERT profiles 2 and 3 and SI Fig. 4). The differences in the resistivities of this layer between profiles 2-4 and 6, 7, 11, 12 (Figs. 6, 8, main text; SI Fig. 4) are due to the different acquisition periods: P2-P4 were measured in autumn after a very dry summer and P6/7 in January during a wet winter. Transects P11 and P12 were measured beginning of June 2023 during an intermediate state of soil wetness conditions. This results in differences in soil saturation and affects the electrical properties of the soil, resulting in lower resistivities in wetter conditions. Therefore, the upper centimetres of the topsoil in P2-P4 are characterized by higher resistivities during dry soil conditions of the topsoil and significantly lower resistivities in the topsoil at P6, P7, P11 and P12.

3.2 Black Floodplain Soil zone

For this zone, it is all the more important to note, that the designation of the near-surface layers and horizons remains rather provisional. In contrast to the neighboring Chernozem zone, the entire area under investigation was completely affected by the ground levelling for the construction of the airfield.

In addition, it has since been heavily built over, so that a 'pristine' standard profile for reference could not yet be identified. In any case, the information we gathered on the properties and distribution of the units encountered here, is regarded sufficiently meaningful both for reconnaissance and prospection purposes.

Stratigraphic Unit 1 (SU1): This Middle Keuper mudstone sequence occurs in this zone as well, displaying congruent properties to those described in section 3.1.1. The respective deposits were exposed in cores EN-RK 1, 32, 33 and 41. In the ERT profiles, this unit is characterized by low resistivity values up to 60 Ωm (Fig. 6 and 8, main text; ERT profiles 2, 3, 6 and 7; Si Fig. 4).

Stratigraphic Unit 6 (SU6): The direct superposition of SU1 is formed by a gravelly sand to sandy gravel with thicknesses varying between ca. 100 and 170 cm and an upper boundary at around 178 m asl. SU6 was encountered in all the boreholes of this zone (Figs. 5 and 9, main text). Its matrix is represented by a mostly yellowish red to (light reddish) brown, poorly-sorted and highly calcareous fine to coarse sand which contains occasional loamy segments ranging from olive to light olive brown and brownish grey (Munsell colors varying from 2,5Y, 10YR, 7,5YR, 5YR to mostly 2,5YR 6/3-5/2). Despite having a fairly similar appearance to SU2, there are numerous indications for a distinction of these two units: (i) The upper boundary of SU6 is usually already within the first meter of the boreholes, meaning that the slope debris (SU3) as well as loess-like deposits (SU4-SU5.1) overlying SU2 are totally absent here. Therefore, a different chronostratigraphic position has to be assumed. (ii) On average, the well-rounded pebbles are noticeably coarser, have higher overall proportions (ca. 30 to 60% of the deposit) and also higher limestone contents compared with SU2, whereas quartz, chert and rhyolite occur equally in both units. (iii) The sandy matrix of SU6 shows a higher carbonate content than SU2, which might, however, be a slightly deceptive observation caused by the bore dust from the limestone-heavier gravel in SU6. (iv) Sporadically, sandy segments low in pebbles are encountered (cores EN-RK 12, 15 and 35) that even show tendencies of small-scale fining-up cycles as documented in core EN-RK 35 between 151 and 200 cm coring depth.

For the mentioned differences to SU2 concerning composition, facies and stratigraphy, we regard SU6 as a clearly independent unit and tentatively interpret it as a Late Weichselian to Early Holocene fluvial gravel. The resistivity values of the SU6 are similar to those of SU2 and are characterized as high-resistivity layer with values up to 400 Ωm (Fig. 6, main text, ERT profile 4).

Stratigraphic Unit 7 (SU7): Overlying SU6 is a black to very dark brown or dark olive brown (Munsell colors 7,5YR 2/1 to 2,5Y 3/1), loamy-clayey deposit with thicknesses ranging from c. 70 up to 120 cm. The sand fraction is fairly well-sorted and dominated by medium to coarse sand, while the proportion of clay can regularly reach 50%. There are no macroscopic bedding features, but in some cases, abrupt

shift towards lighter (brown) (7,5YR 4/3 to 10YR 3/3) and siltier members seem to naturally occur (cores EN-RK 2, 11, 48), especially in the upper half of the unit. Carbonate contents are stratigraphically inconsistent, both within and between the boreholes, they vary from 0% to about 10%. At the lower boundary, the contact zone to SU6 is mostly enriched in stones and coarse pebbles, while the upper part of the SU6 gravels is often still loamy, humic and decalcified, even if the bulk of the SU7 deposits is calcareous (EN-RK 11, 13, 17, 33, 48, 49). Frequently, a downcore gradient of decreasing clay and humus contents and increasing carbonate content can be observed at this lower boundary of SU7, suggesting chemical weathering. Among notable admixtures, apart from occasional pebbles (~5%), SU7 also variably contains potential anthropogenic markers such as charcoal flakes and burnt loam (EN-RK 2, 35, 46, 49). Together with the high thickness and humus contents, this implies a formation as a pedosediment, notwithstanding that at least at the lower boundary indications for in-situ weathering and -pedogenesis seem to exist. Therefore, and on account of its stratigraphic and topographic position, as well as its textural distinctness from the loess-derived topsoil of the chernozem zone, we interpret SU7 as a Holocene overbank deposit and classify it as “Black Floodplain Soil”, henceforth: BFS. Similar to the units SU3-SU5, SU7 is also visible in the ERT profile 4. SU7 has heterogeneously distributed resistivity values of 50 to 100 Ωm.

3.3 Deviations and anomalies

The soil removal during the airfield construction affected especially the central part of the AOI in the chernozem zone, where the chernic horizon and the loess-like deposits are (largely) missing, being replaced by a 20 to 30 cm ploughing horizon often formed in the slope debris of SU3. Relief levelling for the airfield might have led to a certain backfilling of topographic depressions in the Black Floodplain Soil zone, which would explain the occurrence of near-surface siltier layers in that area. However, this interpretation remains hypothetical until we managed to locate a standard profile and also obtained some numerical ages for these cover layers. As of now, we refrain from their interpretation as either colluvial, alluvial or anthropogenic layers. Surprisingly, no unambiguous colluvial layers, defined as the correlate sediment of land use-driven soil erosion, were found in the entire study area, at all yet – neither at the foot slope of Roter Berg, nor elsewhere.

For some positions we could assume existence of occupation layers or other subsurface archaeological features, such as pits, based on a combination of conspicuous sediment characteristics. Among those are abrupt changes in color, structure and carbonate content, excessive thickness of the humic solum and artificial constituents in the form of pottery sherds, burnt loam or the accumulation of charcoal fragments. This applies to 9 cores located within the chernozem zone, namely EN-RK 19-21, RK 25, 27, 38, 42, 55 and 56, as well as core EN-RK 48 in the BFS zone (see Figs. 3, 5, 9, main text) the usual depth of these features below the surface amounts to <1.5 m.

Supplementary Section 4 – Additional Electrical Resistivity Tomography data

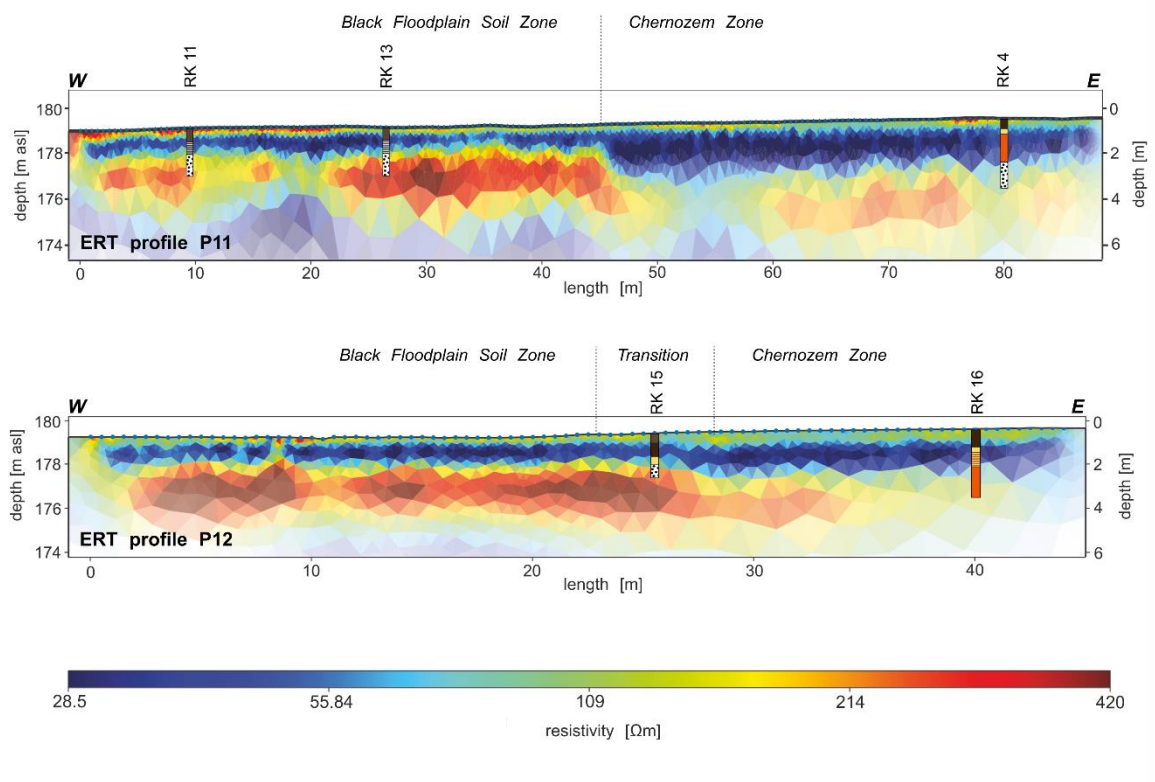

SI Fig. 4: ERT-profiles P11 and P12 (electrode spacing of 0.5 m, model is based on a joint inversion of a Wenner and Dipole-Dipole configuration). For positioning, see Figs. 3 and 9 in the main text. For pedostratigraphic symbology, see Fig. 5, main text.

A direct comparison of the ERT profiles of the two main soil units reveals that in the area of the black alluvial soils (P2 from RK 41, P4, P11, P12) (Fig. 8, main text, SI Fig. 4) the overburden on the gravel has a lower thickness and the gravel layer appears to be slightly higher in absolute terms. Furthermore, the sediment layers from SU3-SU5 and SU7 appear as an almost uniform low-resistivity layer, and it is not possible to distinguish between the different soil materials. The differences in the resistivities of this layer between profiles 2-4 and 6, 7, 11, 12 are due to the different acquisition periods: P2-P4 were measured in autumn after a very dry summer and P6/7 in January during a wet winter. Transects P11 and P12 were measured beginning of June 2023 during an intermediate state of soil wetness conditions. This results in differences in soil saturation and affects the electrical properties of the soil, resulting in lower resistivities in wetter conditions. Moreover, the upper centimetres of the topsoil in P2-P4 are characterized by higher resistivities during dry soil conditions of the topsoil and significantly lower resistivities in the topsoil at P6, P7, P11 and P12.

The ERT profiles 2-4 are located in the section of the forest along the central drilling transects T1-T3 and are displayed in Figure 6 in the main text. Profiles 6 and 7 are next to P3 and P 11/12 in the south of the AOI. The Keuper mudstone encountered in SU1 is characterised by low resistivities (up to 50 Ωm) at a depth of 4m in P2-4 and P6/7 (Figs. 6 and 8, main text) as well in P11 (SI Fig. 4). In profile P12

(SI Fig. 4), the Keuper mudstone is less pronounced. The ERT surveys clearly show the gravel of SU2 with higher resistivities and a thickness of up to 2 m. In particular, the upper boundary of this layer corresponds very well with the depth delimitation from the sediment cores. The SU2 layer appears almost constant over the entire length of the profiles at a depth of approximately 2 metres. The same applies to unit SU6 in ERT profile 4 (Fig. 6, main text).

Based on the resistivity values, only profiles P6/7 and P11 show clear anomalies in SU2. P6 shows a breakout of the layer with resistivities > 200 Ωm towards the surface. This anomaly is located approximately in the middle of the profile. At P7, from profile metre 15, there is an offset of approximately 2m in the SU2 layer towards the ground surface.

P11 on the other hand, shows an offset of SU2 towards SU1 at approx. 45 m. In P12 the SU2 expires to the east, following the decreasing resistivity values. The overlying sediment layers of loess, loamy slope sediment, humus- and clay-rich high flood sediments (SU3-SU5 and SU7) are characterised by significantly lower resistivities. In P3, P6, P7 and at the beginning of P2 and P4 the layers of SU3-SU7 are recognisable as low resistance layer with varying values from 50 – 100 Ωm. In ERT profiles 11 and 12, however, this layer is even more clearly demarcated with lower resistances (28.5 – 50 Ωm). Following the offset of the gravel layer SU2, the layer thickness increases according. The sediment layers from SU3-SU5 and SU7 appear as an almost uniform layer of lower resistivity values, and it is not possible to distinguish between the different soil materials. However, the differences in the resistivities of this layer between profiles 2-4 and 6,7,11,12 are due to the different acquisition periods: P2-P4 were measured in autumn after a very dry summer and P6/7 in January during a wet winter and P11/12 in in the following June. This results in differences in soil saturation and affects the electrical properties of the soil, resulting in lower resistivities in wetter conditions. Moreover, the upper centimetres of the topsoil in P2-P4 are characterized by higher resistivities of the dry soil and significantly lower resistivities in the topsoil at P6, P7, P11 and P12. In a direct comparison between the ERT profiles of both main soil units, it is noticeable that in the area of the black alluvial soils (P2, P4, P11 and P12) the overlay on the gravel has a lower thickness and the gravel layer appears to be somewhat higher in absolute terms.

Supplementary Section 5 – Dating and additional archaeological information

5.1 Detailed information on dating approaches

We recovered a total of 14 pottery sherds from the sediment cores in Neuses. They are catalogued under the TLDA (Thuringian State Department for the Preservation of Monuments and Archaeology) procedure/inventory number *22/220*. Their description is presented below. Generally, their high degree of fragmentation due to the coring procedure complicates the chronological classification. Therefore, the pottery-based chronological assessment only cautiously be used as a *terminus post quem* for the interpretation of the respective sediment layers. Specimens might also have been introduced into the deposits via bioturbation or through the coring procedure itself.

Fz.no. 201501: Sondage; RK 25, 119 cm von GOK (inv.-No. 22/220-9)
A freshly-broken wall sherd; reduction-fired, black, hand-built ware; surface well preserved; medium-grained quartz; soft-fired; 1.9x 2.6cm, thickness 0.7 cm; dating: prehistoric
Fz.No. 201502: Sondage; RK 32, 85 cm von GOK (inv.-No. 22/2202-7)
Heavily fragmented ceramic fragment; reduction-fired, hand-built earthenware; soft-fired; 0.4x0.7 cm, thickness 0.3 cm; dating: prehistoric
FZ.no. 201503: Sondage; RK 48, 55 cm from GOK (inv.-No. 22/220 - 8)
Heavily fragmented wall sherd; probably from a vessel; red brick-like ware with even fine grain and smooth surface; hard-fired; traces of manufacture not visible; surface preserved on one side; approx. 1.5 x 0.9 cm, thickness 0.5 cm; dating: probably medieval
Fz.No. 201504: Sondage; RK 35, 80 cm von GOK (inv.-N0. 22/220-10)
Fragmentary wall sherd; reduction-fired, black, hand-built ware; well-preserved rough surface, medium-coarse quartz grain; medium-hard fired; 0.9x2.4 cm, thickness 0.6 cm; dating: prehistoric
FZ.no. 201505: Sondage; RK 47, 41 cm from GOK (inv. no. 22/220 - 6)
Heavily fragmented wall sherd; rough-walled, reduction-fired, grey ware with a quartz grain and little mica; hard-fired; traces of manufacture not visible; surfaces well preserved; approx. 1.4 x 1.5 cm, thickness 0.4 cm; dating: medieval
FZ.no. 201506: Sondage; RK 48, 38 cm from GOK (inv.-No. 22/220 - 5)
a. Heavily fragmented, freshly broken, wall sherd; probably from miniature vessel; reducing grey fired wheel thrown ware with yellow oxidising fired outer surface; fine leanness; hard fired; 1.5 x 1.9 cm, thickness 0.3-0.4 cm; dating: medieval
b. Heavily fragmented wall sherd; grey, reduction-fired ware with mantled orange surface; medium coarse grain of quartz and mica; moderately hard-fired; 0.7 x 0.8 cm, thickness 0.5 cm; dating: indeterminable (prehistoric-medieval)
FZ.no. 201507: Sondage; RK 27, 65 cm from GOK (inv. no. 22/220 - 3)

Heavily fragmented wall sherd; oxidisingly fired, yellow to reddish, younger wheel thrown ware with green lead glaze on the inside; finely tempered, occasional mica; hard fired; 1.4 x 1.9 cm, thickness 0.5 cm; dating: Late Middle Ages, probably 14th/15th century

Fz.No. 201508: Sondage; RK 46, 53cm von GOK (inv.-No. 22/220-2)

Heavily fragmented wall sherd; reduction-fired, black, hand-agglomerated ware; medium to coarse quartz grain; soft-fired; 0.8x1.1 cm, thickness 0.4 cm; dating: prehistoric

FZ.no. 201509: Sondage; RK 38, 36 cm from GOK (inv. no. 22/220 - 1)

a. Heavily fragmented ceramic fragment; red brick-like ware with uniform fine grain and smooth surface; hard-fired; traces of manufacture not visible; surface preserved on one side; approx. 0.7 x 0.8 cm, thickness 0.2 cm; dating: indeterminable (medieval/modern period)

b. Heavily fragmented wall sherd, freshly broken; grey-white earthenware with white glaze, probably faience; hard-fired; wheel-thrown ware; surface preserved in fragments; fine grain; 0.8 x 0.9 cm, thickness 0.2 cm; dating: modern period

FZ.no. 201510: Sondage; RK 32, 45 cm from GOK (inv. no. 22/220 - 4)

Heavily fragmented wall sherd; reduction-fired, hand-built ware; orange engobe on the inside; coarse grain with quartz and lime; soft-fired; heavily rolled; 1 x 1.1 cm, thickness 0.5 cm; dating: indeterminable (Prehistoric/High Middle Ages)

FZ.no. n.a.: Sondage; RK 57: 40-50 cm von GOK (inv.-no. 22/220-11)

a. One rim sherd and two heavily fragmented wall sherds; reduction-fired black hand-built ware with smoothed surface; coarse lime lean; soft to moderately hard-fired; simple straight rim with slightly convex end, rim diameter 4-6 cm, 1.9 x 2 cm, thickness 0.7 cm; WS fragments 0.9 x 1.1 cm, 0.7 x 1.1 cm; dating: prehistoric

b. Heavily fragmented wall sherd; oxidisingly-fired wheel thrown ware; black lead glaze inside, surface poorly preserved outside; 0.9 x 1.1 cm, thickness 0.5 cm; dating: modern period

SI Tab. 1: Data and results for all samples subjected to radiocarbon dating.

Lab Nr MAMS	Sample ID core/depth [cm]	^{14}C Age [yr BP]	±	δ^{13}C AMS [‰]	Probability 68% (1σ)	Probability 95% (2σ)	C:N	C [%]	Collagen [%]	Material
60280	*RK55/260*	*608*	*22*	*-22.4*	*cal AD 1309-1396*	*cal AD 1302-1401*	*3.2*	*37.3*	*4.4*	*bone*
60281	RK55/154	919	23	-20.7	cal AD 1046-1165	cal AD 1038-1204		55.0		charcoal
60282	RK53/40	941	23	-21.4	cal AD 1042-1156	cal AD 1035-1160		69.1		charcoal
60284	RK21/139	835	25	-29.6	cal AD 1179-1260	cal AD 1169-1265		61.6		charcoal
65026	*RK56/180*	*617*	*17*	*-24.4*	*cal AD 1305-1393*	*cal AD 1301-1398*	*3.2*	*42.4*	*7.3*	*bone*
65027	RK56/243	5533	32	-34.1	cal BC 4442-4342	cal BC 4447-4337				charcoal
					Calibrated Ages					

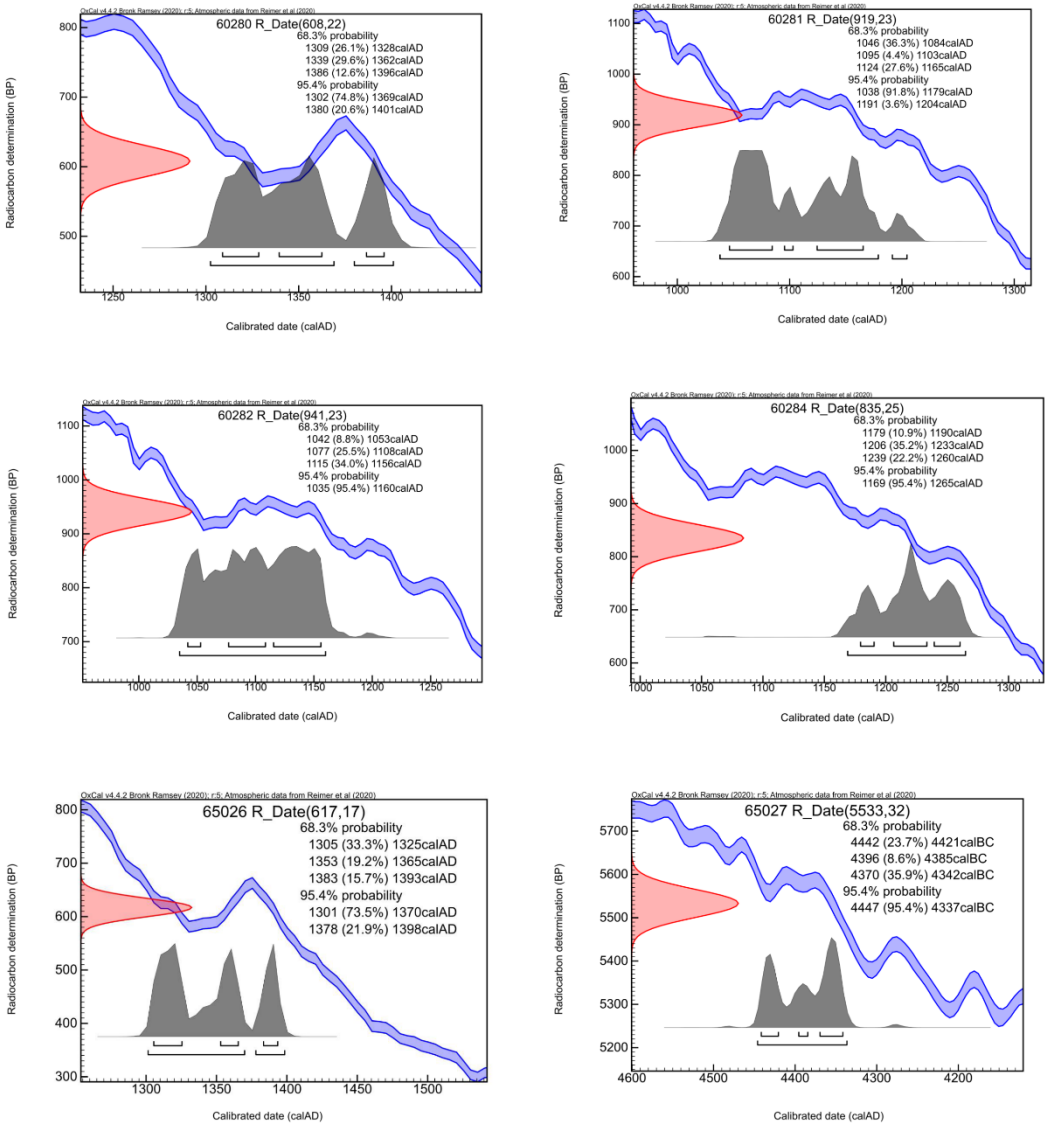

SI Fig. 5: Calibration graphs of all samples subjected to radiocarbon dating. Calibration was done using OXCal v.4.4.2 and the IntCal20 curve (Reimer et al, 2020) (2)

.

5.2 Archaeological evidence for the position of the cemetery within the village

We argue that the course of the boundary between the Chernozem and Black Floodplain Soil zone had a bearing not only on the positioning but also on the internal structure of the village: During the 1926/27 excavation, a wall fragment of 25 meters length was discovered south of the cemetery, beyond which, no occupation features were found to the south. Accordingly, it was interpreted as part of the cemetery enclosure forming the southernmost branch of the village (3). The 2012 excavation uncovered another wall fragment with a length of <3 meters at the very northern limit of the excavated area, which was assumed to turn northwards from its eastern edge (Fig. 9, main text). In many aspects these two remnants are strikingly similar to each other: (i) building material – undressed chunks of limestone and greenish sandstone, (ii) orientation and position – nearly W-E oriented, parallel to "Weg zum Roten Berg" in ~40 m distance, as well as (iii) age – tentatively late medieval. Only the thickness (60 cm v. 80 cm) is where the two walls slightly differ (3–5). Therefore, it seems plausible to regard the 2012 wall as the eastern continuation of the one from 1926/27. Unlike the 1926/27 excavation, the more easterly 2012 excavation detected numerous medieval occupation features *south* of this wall, as well, where also the Chernozem Zone extents further to the south (Fig. 9, main text).

5.3 Anthropological information

SI Tab. 2: Characterization of the bone fragments found in the sediment cores. Abbreviations: dx=sin refers to an ambiguous dextral or sinistral position, M=F to an ambiguous sex estimation of the specimen. The age-at-death indications are given in the description column as an age range/minimum age or as a developmental stage (e.g. adult). The two bones sampled for ^{14}C dating are indicated and the CEZA lab codes are specified. All bones are stored at the TLDA in Weimar.

Core EN-…	Depth [cm]	Inv.No.	Species	Skeletal Region	Description	Dating Lab code
RK20	55	**22/220-18**	non-human	-	one tiny fragment of an animal bone; species, sex and age-at-death not determinable	-
RK55	237	**22/220-19**	human	pelvis?	few tiny fragments of cortical and spongy bone; adult; M=F	-
RK55	260	**22/220-13**	human	skull	several fragments of neurocranium, probably one individual; 20-40 years; M=F	MAMS 60280
RK55	260	**22/220-14**	human	skull	few neurocranium fragments, two orbit roof fragments, possibly same individual as -13, similar morphology; 20-40 years; M=F	-
RK55	264	**22/220-12**	human	lower arm	proximal shaft fragment of an ulna (dx=sin); 45+ years; M=F	-
RK55	264	**22/220-15**	human	leg	few fragments of robust compact bone, likely femur or tibia; 20-50 years; M=F	-
RK55	270	**22/220-16**	human	-	tiny fragment of cortical bone; adult; M=F	-
RK55	272	**22/220-17**	human	arm	fragment of trochlea humeri; adult; M=F	-
RK56	180	**22/220-20**	human	foot	Fragments of left first metatarsal with proximal phalanx and one shaft fragment of another metatarsal; 20-50 years; M=F	MAMS 65026

6. Stratigraphic logs of sediment cores

.

SI Tab. 3: Stratigraphic logs of all sediment cores retrieved in the study area. Coordinates are given in UTM zone 32N

Core EN-RK 1 (642451.13 E, 5654013.3 N)		
Depth (cm)	**Strat. Unit**	**Selected Properties**
0-75	SU7	loamy, humic, calcareous
75-230	SU6	sandy-gravelly, calcareous
230-400	SU1/SU3	silty-clayey, slightly calcareous

Core EN-RK 2 (642481.52 E, 5654016.55 N)		
Depth (cm)	**Strat. Unit**	**Selected Properties**
0-90	SU7	loamy, humic, calcareous
90-270	SU6	sandy-gravelly, calcareous
270-300	SU1/SU3	silty-clayey, slightly calcareous

Core EN-RK 3 (642577.87 E, 5654052.44 N)		
Depth (cm)	**Strat. Unit**	**Selected Properties**
0-55	SU5.2	silty, humic, calcareous
55-75	SU5.1	silty, calcareous
75-255	SU3	loamy, calcareous
255-300	SU2	sandy-gravelly, calcareous

Core EN-RK 4 (642603.29 E, 5654042.24 N)		
Depth (cm)	**Strat. Unit**	**Selected Properties**
0-45	SU5.2	silty, humic, calcareous
45-67	SU5.1	silty, calcareous
67-190	SU3	loamy, calcareous
190-300	SU2	sandy-gravelly, calcareous

Core EN-RK 5 (642486.16 E, 5654271.1 N)		
Depth (cm)	**Strat. Unit**	**Selected Properties**
0-75	SU5.2	silty, humic, calcareous
75-127	SU5.1	silty, calcareous
127-180	SU4	silty to loamy, calcareous
180-500	SU3	loamy to silty, calcareous

Core EN-RK 6 (642472.07 E, 5654193.51 N)		
Depth (cm)	**Strat. Unit**	**Selected Properties**
0-55	SU5.2	silty, humic, calcareous
55-85	SU5.1	silty, calcareous
85-200	SU3	loamy, calcareous

Core EN-RK 7 (642510.24 E, 5654189.61 N)		
Depth (cm)	**Strat. Unit**	**Selected Properties**
0-60	SU5.2	silty, humic, calcareous
60-86	SU5.1	silty, calcareous
86-165	SU4	silty to loamy, calcareous
165-332	SU3	loamy to silty, calcareous
332-400	SU2	sandy-gravelly, calcareous

Core EN-RK 8 (642519.3 E, 5654246.53 N)		
Depth (cm)	**Strat. Unit**	**Selected Properties**
0-90	SU5.2	silty, humic, slightly calcareous, colluvial influence(?)
90-145	SU5.1	silty, calcareous
145-200	SU3	loamy, calcareous

Core EN-RK 9 (642558.03 E, 5654185.82 N)		
Depth (cm)	**Strat. Unit**	**Selected Properties**
0-90	SU5.2	silty, humic, slightly calcareous, colluvial influence(?)
90-136	SU5.1	silty, calcareous
136-152	SU4	silty to loamy, calcareous
152-200	SU3	loamy to silty, calcareous

Core EN-RK 10 (642566.33 E, 5654231.9 N)		
Depth (cm)	**Strat. Unit**	**Selected Properties**
0-100	SU5.2	silty, humic, slightly calcareous, colluvial influence(?)
100-135	SU5.1	silty, calcareous
135-155	SU4	silty to loamy, calcareous
155-200	SU3	loamy, calcareous

Core EN-RK 11 (642538.81 E, 5654013.62 N)		
Depth (cm)	**Strat. Unit**	**Selected Properties**
0-95	SU7	loamy, humic, slightly- to non-calcareous
95-200	SU6	sandy-gravelly, calcareous

Core EN-RK 12 (642560.21 E, 5654038.18 N)		
Depth (cm)	**Strat. Unit**	**Selected Properties**
0-85	SU7	loamy to silty, humic, calcareous
85-200	SU6	sandy-gravelly, calcareous

Core EN-RK 13 (642555.59 E, 5654018.08 N)		
Depth (cm)	**Strat. Unit**	**Selected Properties**
0-100	SU7	loamy to silty, humic, slightly calcareous
100-200	SU6	sandy-gravelly, calcareous

Core EN-RK 14 (642545.59 E, 5654066.3 N)		
Depth (cm)	**Strat. Unit**	**Selected Properties**
0-120	SU7	loamy to silty, humic, calcareous
120-200	SU6	sandy-gravelly, calcareous

Core EN-RK 15 (642549.16 E, 5654073.45 N)		
Depth (cm)	**Strat. Unit**	**Selected Properties**
0-112	SU7/SU5.2	silty to loamy, humic, calcareous, reworked(?)
112-140	SU7/SU5.1	silty to loamy, calcareous, reworked(?)
140-200	SU6	sandy-gravelly, calcareous

Core EN-RK 16 (642563.39 E, 5654076.95 N)		
Depth (cm)	**Strat. Unit**	**Selected Properties**
0-70	SU5.2	silty, humic, slightly calcareous, colluvial influence(?)
70-90	SU5.1	silty to fine-sandy, calcareous
90-150	SU4	silty to loamy, more gravelly than elsewhere, calcareous
150-200	SU3	loamy-clayey, slightly gravelly, highly calcareous

Core EN-RK 17 (642497.66 E, 5654059.73 N)		
Depth (cm)	**Strat. Unit**	**Selected Properties**
0-125	SU7	loamy-clayey to silty, humic, calcareous
125-200	SU6	sandy-gravelly, calcareous

Core EN-RK 18 (642617.92 E, 5654177.53 N)		
Depth (cm)	**Strat. Unit**	**Selected Properties**
0-75	SU5.2	silty, humic, slightly calcareous, colluvial influence(?)
75-137	SU5.1	silty, calcareous
137-163	SU4	silty to loamy, calcareous
163-200	SU3	loamy-clayey, slightly gravelly, calcareous

Core EN-RK 19 (642470.4 E, 5654171.66 N)		
Depth (cm)	**Strat. Unit**	**Selected Properties**
0-89	SU5	silty, humic, slightly calcareous, occupation feature
89-159	SU4	silty to loamy, calcareous
159-263	SU3	loamy-clayey, calcareous
263-300	SU2	sandy-gravelly, calcareous

Core EN-RK 20 (642504.19 E, 5654163.18 N)		
Depth (cm)	**Strat. Unit**	**Selected Properties**
0-115	SU5	silty, humic, slightly calcareous, occupation feature
115-130	SU5.1	silty, calcareous
130-160	SU4	silty to loamy, calcareous
160-200	SU3	loamy-clayey, calcareous

Core EN-RK 21 (642550.98 E, 5654144.26 N)		
Depth (cm)	**Strat. Unit**	**Selected Properties**
0-124	SU5	silty, humic, slightly calcareous, occupation feature
124-142	SU5.1	silty, calcareous
142-195	SU4	silty to loamy, calcareous
195-300	SU3	loamy-clayey, calcareous

Core EN-RK 22 (642549.98 E, 5654138.02 N)		
Depth (cm)	**Strat. Unit**	**Selected Properties**
0-30	SU5	silty, slightly humic, calcareous, ploughing horizon
30-57	SU5.1	silty, calcareous
57-95	SU4	silty to loamy, calcareous
95-200	SU3	loamy-clayey, calcareous

Core EN-RK 23 (642507.051 E, 5654173.244 N)		
Depth (cm)	**Strat. Unit**	**Selected Properties**
0-60	SU5.2	silty, humic, calcareous
60-93	SU5.1	silty, calcareous
93-157	SU4	silty to loamy, calcareous
157-200	SU3	loamy-clayey, calcareous

Core EN-RK 24 (642506.04 E, 5654170.094 N)		
Depth (cm)	**Strat. Unit**	**Selected Properties**
0-65	SU5.2	silty, humic, calcareous
65-95	SU5.1	silty, calcareous
95-163	SU4	silty to loamy, calcareous
163-200	SU3	loamy-clayey, calcareous

Core EN-RK 25 (642551.031 E, 5654170.094 N)		
Depth (cm)	**Strat. Unit**	**Selected Properties**
0-143	SU5	silty, humic, slightly calcareous, occupation feature
143-166	SU4	silty to loamy, calcareous
166-200	SU3	loamy-clayey, calcareous

Core EN-RK 26 (642551.407 E, 5654165.83 N)		
Depth (cm)	**Strat. Unit**	**Selected Properties**
0-63	SU5.2	silty, humic, calcareous
63-130	SU5.1	silty, calcareous
130-160	SU4	silty to loamy, calcareous
160-200	SU3	loamy-clayey, slightly gravelly, calcareous

Core EN-RK 27 (642552.307 E, 5654161.624 N)		
Depth (cm)	**Strat. Unit**	**Selected Properties**
0-105	SU5	silty, humic, slightly calcareous, occupation feature
105-185	SU4	silty to loamy, calcareous
185-200	SU3	loamy-clayey, slightly gravelly, calcareous

Core EN-RK 28 (642507.336 E, 5654175.534 N)		
Depth (cm)	**Strat. Unit**	**Selected Properties**
0-57	SU5.2	silty, humic, calcareous
57-89	SU5.1	silty, calcareous
89-100	SU4	silty to loamy, calcareous

Core EN-RK 29 (642599.314 E, 5654129.678 N)		
Depth (cm)	**Strat. Unit**	**Selected Properties**
0-75	SU5.2	silty, humic, slightly calcareous
75-100	SU5.1	silty, calcareous
100-180	SU4	silty to loamy, calcareous
180-200	SU3	loamy-clayey, gravelly, calcareous

Core EN-RK 30 (642592.161 E, 5654130.277 N)		
Depth (cm)	**Strat. Unit**	**Selected Properties**
0-100	SU5/5.2	silty, humic, calcareous, colluvial/occupation feature(?)
100-140	SU5.1	silty, calcareous
140-180	SU4	silty to loamy, calcareous
180-200	SU3	loamy-clayey, slightly gravelly, calcareous

Core EN-RK 31 (642590.426 E, 5654130.207 N)		
Depth (cm)	**Strat. Unit**	**Selected Properties**
0-118	SU5	silty, humic, slightly calcareous, occupation feature
118-137	SU5.1	silty, calcareous
137-168	SU4	silty to loamy, calcareous
168-200	SU3	loamy-clayey, gravelly, calcareous

Core EN-RK 32 (642479.14 E, 5654117.471 N)		
Depth (cm)	**Strat. Unit**	**Selected Properties**
0-210	SU7/SU6	loamy-clayey, gravelly, calcareous, modern arch. feature
210-245	SU6	sandy-gravelly, (slightly) calcareous
245-300	SU1	clayey-silty, non-calcareous

Core EN-RK 33 (642479.596 E, 5654109.423 N)		
Depth (cm)	**Strat. Unit**	**Selected Properties**
0-110	SU7	loamy-clayey to silty, humic, highly calcareous
110-295	SU6	sandy-gravelly, calcareous
295-300	SU1	clayey-silty, non-calcareous

Core EN-RK 34 (642479.371 E, 5654119.557 N)		
Depth (cm)	**Strat. Unit**	**Selected Properties**
0-120	SU7	loamy-clayey to silty, humic, calcareous
120-170	SU6	sandy-gravelly, calcareous

Core EN-RK 35 (642484.812 E, 5654126.499 N)		
Depth (cm)	**Strat. Unit**	**Selected Properties**
0-100	SU7(?)	silty to loamy-clayey, humic, calcareous, occup. feature (?)
100-200	SU6	sandy-gravelly, calcareous

Core EN-RK 36 (642487.877 E, 5654130.502 N)		
Depth (cm)	**Strat. Unit**	**Selected Properties**
0-20	SU3 (?)	clayey-silty, slightly humic, calcareous, ploughing horizon
20-75	SU3 (?)	clayey-silty, calcareous, secondarily reworked(?)
75-270	SU2/(SU6)	sandy-gravelly, calcareous
270-300	SU1	clayey-silty, non-calcareous

Core EN-RK 37 (642499.156 E, 5654140.447 N)		
Depth (cm)	**Strat. Unit**	**Selected Properties**
0-26	SU3	loamy, slightly humic, calcareous, ploughing horizon
26-169	SU3	loamy to silty, slightly gravelly, calcareous
169-300	SU2	sandy-gravelly, calcareous

Core EN-RK 38 (642497.841 E, 5654123.597 N)		
Depth (cm)	**Strat. Unit**	**Selected Properties**
0-56	SU3(?)	loamy-clayey, humic, calcareous, occupation feature(?)
56-133	SU3	loamy to silty, slightly gravelly, calcareous
133-200	SU2	sandy-gravelly, calcareous

Core EN-RK 39 (642500.037 E, 5654129.742 N)		
Depth (cm)	**Strat. Unit**	**Selected Properties**
0-33	SU3/SU4	loamy-silty, humic, calcareous, ploughing horizon
33-100	SU3	loamy to silty, slightly gravelly, calcareous

Core EN-RK 40 (E, N)		
Depth (cm)	**Strat. Unit**	**Selected Properties**
0-50	SU3/SU4	loamy-silty, humic, calcareous, plough. horiz./ occ. feature
50-144	SU3	loamy-clayey to silty, slightly gravelly, calcareous
144-200	SU2	sandy-gravelly, calcareous

Core EN-RK 41 (642493.404 E, 5654110.005 N)		
Depth (cm)	**Strat. Unit**	**Selected Properties**
0-100	SU7	loamy-clayey, humic, slightly gravelly, calcareous
100-218	SU6	sandy-gravelly, (slightly) calcareous
218-300	SU1	clayey-silty, non-calcareous

Core EN-RK 42 (642497.195 E, 5654119.712 N)		
Depth (cm)	**Strat. Unit**	**Selected Properties**
0-62	SU3/SU4	loamy-clayey, humic, calcareous, occupation feature
62-145	SU3	loamy-clayey, slightly gravelly, calcareous
145-200	SU2	sandy-gravelly, calcareous

Core EN-RK 43 (642499.981 E, 5654134.604 N)		
Depth (cm)	**Strat. Unit**	**Selected Properties**
0-30	SU3/SU4	loamy-clayey to silty, calcareous, ploughing horizon
30-100	SU3	loamy-clayey, calcareous

Core EN-RK 44 (642499.614 E, 5654137.583 N)		
Depth (cm)	**Strat. Unit**	**Selected Properties**
0-30	SU3/SU4	loamy-clayey to silty, calcareous, ploughing horizon
30-100	SU3	loamy-clayey, calcareous

Core EN-RK 45 (642499.725 E, 5654138.506 N)		
Depth (cm)	**Strat. Unit**	**Selected Properties**
0-30	SU3/SU4	loamy-clayey to silty, calcareous, ploughing horizon
30-100	SU3	loamy-clayey, calcareous

Core EN-RK 46 (E, N)		
Depth (cm)	**Strat. Unit**	**Selected Properties**
0-120	SU7	loamy-clayey, humic, (slightly) calcareous
120-200	SU6	sandy-gravelly, calcareous

Core EN-RK 47 (642466.036 E, 5654132.147 N)		
Depth (cm)	**Strat. Unit**	**Selected Properties**
0-89	SU7	loamy-clayey to silty, humic, calcareous, occupation feature
89-160	SU6	sandy-gravelly, (slightly) calcareous

Core EN-RK 48 (642465.437 E, 5654124.415 N)		
Depth (cm)	**Strat. Unit**	**Selected Properties**
0-100	SU7	loamy-clayey, humic, slightly calcareous, occ. feature
100-200	SU6	sandy-gravelly, calcareous

Core EN-RK 49 (642464.651 E, 5654117.562 N)		
Depth (cm)	**Strat. Unit**	**Selected Properties**
0-90	SU7	loamy-clayey, humic, (slightly) calcareous
90-200	SU6	sandy-gravelly, calcareous

Core EN-RK 50 (642467.611 E, 5654152.219 N)		
Depth (cm)	**Strat. Unit**	**Selected Properties**
0-84	SU7(?)	loamy-clayey, humic, calcareous
84-172	SU3	loamy-clayey, calcareous
172-200	SU2	sandy-gravelly, calcareous

Core EN-RK 51 (642549.05 E, 5654133.59 N)		
Depth (cm)	**Strat. Unit**	**Selected Properties**
0-34	SU5	silty, (slightly) humic, calcareous, ploughing horizon
34-50	SU5.1	silty, calcareous
50-95	SU4	silty to loamy, calcareous
95-186	SU3	loamy-clayey, calcareous
186-300	SU2	sandy-gravelly, calcareous

Core EN-RK 52 (642549.233 E, 5654124.373 N)		
Depth (cm)	**Strat. Unit**	**Selected Properties**
0-38	SU5.1/SU4	silty, (slightly) humic, calcareous, ploughing horizon
38-72	SU4	silty to loamy, calcareous
72-100	SU3	loamy-clayey, calcareous

Core EN-RK 53 (642547.256 E, 5654112.041 N)		
Depth (cm)	**Strat. Unit**	**Selected Properties**
0-43	SU5.1/SU4	silty, (slightly) humic, calcareous, ploughing horizon
43-81	SU4	silty to loamy, calcareous
81-173	SU3	loamy-clayey, calcareous
173-200	SU2	sandy-gravelly, calcareous

Core EN-RK 54 (642548.551 E, 5654118.275 N)		
Depth (cm)	**Strat. Unit**	**Selected Properties**
0-44	SU5.1/SU4	silty, (slightly) humic, calcareous, ploughing horizon
44-83	SU4	silty to loamy, calcareous
83-100	SU3	loamy-clayey, calcareous

Core EN-RK 55 (642538.479 E, 5654119.482 N)		
Depth (cm)	**Strat. Unit**	**Selected Properties**
0-285	SU2-SU5	loamy-silty to gravelly, calcareous, slightly humic, occupation feature (mass grave)
285-347	SU2	sandy-gravelly, calcareous
347-400	SU1	clayey-silty, non-calcareous

Core EN-RK 56 (642538.228 E, 5654116.3 N)		
Depth (cm)	**Strat. Unit**	**Selected Properties**
0-270	SU2-SU5	loamy-silty to gravelly, calcareous, slightly humic, occupation feature (mass grave)
270-300	SU2	sandy-gravelly, calcareous

Core EN-RK 57 (642491.878 E, 5654188.932 N)		
Depth (cm)	**Strat. Unit**	**Selected Properties**
0-71	SU5.2	silty, humic, calcareous
71-100	SU4	silty to loamy, calcareous
100-331	SU3	loamy-clayey, calcareous
331-500	SU2	sandy-gravelly, calcareous

Core EN-RK 58 (642526.299 E, 5654186.671 N)		
Depth (cm)	**Strat. Unit**	**Selected Properties**
0-76	SU5.2	silty, humic, calcareous
76-100	SU5.1	silty, calcareous
100-168	SU4	silty to loamy, calcareous
168-320	SU3	loamy-clayey, calcareous
320-530	SU2	sandy-gravelly, calcareous
530-600	SU1	clayey-silty, non-calcareous

References Supplementary Information

Bolle, M. Die Wüstung Neuses am Roten Berg: Ein Beitrag zur Siedlungskunde mit 2 Tafeln und 2 Skizzen. Jahrb Akad Gemeinnütziger Wiss Zu Erf NF. 1937; 53:57–85.

Krauße, Lars. Ausgrabung “Zum Zoopark” in Erfurt von Mai bis August 2012. Weimar: Thuringian State Office for Monument Preservation and Archaeology; 2012 p. 1–5. Report No.: VG-Nr.: 12/107.

Sczech K. Stadtarchäologischer Bericht über das Jahr 2012. Mitteilungen Ver Für Gesch Altertumskunde Von Erf NF 21. 2012;74:125–46.

Seidel G, editor. Geologie von Thüringen: mit 34 Tabellen. 2., neubearbeitete Auflage. Stuttgart: E. Schweizerbart’sche Verlagsbuchhandlung (Nägele u. Obermiller); 2003. 601 p.

Reimer PJ. Composition and consequences of the IntCal20 radiocarbon calibration curve. Quat Res [Internet]. 2020 Jul [cited 2023 Oct 1];96:22–7. Available from: https://www.cambridge.org/core/product/identifier/S0033589420000423/type/journal_article